

Zero-Point Forces in Acoustic Waves

Laurence J. November

La Luz Physics, La Luz NM 88337-0217 USA

laluzphys@yahoo.com

May 24, 2019

Abstract

By the acousto-optic effect, an acoustic plane wave produces a 1D index-of-refraction or permittivity wave variation through a medium. But adjacent material planes of alternating permittivity should interact due to the zero-point (ZP) field to produce internal forces, roughly like the Casimir effect in a stack of regularly spaced discrete conducting plates. The ZP force in a smoothly varying 1D permittivity wave is modeled and found to consist mainly of bulk repulsive and double-wavenumber harmonics. It is stronger than the Casimir ZP attractive force in the corresponding discrete alternating-layer stack at all physically meaningful repetition scales, extends to larger scales, falling off universally only as the inverse square of the wavelength, and shows no temperature sensitivity. Thus, at its extremes, a standing acoustic wave exhibits a bulk expansive ZP pressure through the material volume, but as it passes through its null the ZP pressure vanishes, giving a body stress modulated at twice the acoustic wave frequency. But such repeated tensing in a piezo material is a usual energy-harvesting scenario, suggesting that ZP energy transfer may occur naturally with standing acoustic waves in a piezo medium. A voltage effect is predicted for biphonon lattice vibrations in piezo crystals with the possibility of ‘crystal power’, the extraction of electrical ZP energy across the crystal volume.

keywords: Lifshitz theory of Casimir effect; zero-point thermodynamics; quantum optics;qed; acousto-optical devices.

1 Introduction

Casimir and Polder (Casimir & Polder 1948; Casimir 1948) predicted that discrete closely spaced uncharged parallel conducting plates in a vacuum should exhibit a force of attraction. The ‘Casimir effect’ arises due to the distribution of electromagnetic fluctuations in the background quantum ZP field conditioned by the flat parallel-plate conductors.

It might seem that with such ZP forces, parallel conducting plates should require for their separation at least the energy made available in their attraction. Many physical processes might be said to *borrow* intrinsic energy with the system restored to the original free state with the resupplying of the same quantity of energy that was abstracted, as in the propelling of a vehicle against gravity, or in the warming of a liquid in provision of its latent heat of vaporization for the separating of condensed atoms brought together by ZP forces. However, unlike gravity or passive ZP effects, the ZP force between parallel plates can be turned on or off with tunably conductive, e.g. semiconductor plates, so it actually may *not* always similarly symmetrically cycle the ZP energy:

If parallel tunably conductive plates operate elastically as against a spring-like material between them, the work done in their attraction when the Casimir force is turned on may be much more than what is needed to drive their subsequent separation when the Casimir force is turned off. Energy requirements for the switching process over a cycle should not be related to the strength of the ZP compression, as the separation scale is the single most important property determining the strength of the ZP force. Thus, in principle, it should be possible to design an experiment that takes some energy from the ZP field in each compression cycle.

Various possibilities for the extraction of ZP energy have been put forward based upon different physical effects (Forward 1984; Pinto 1999, 2008; Maclay 2000; Feigel 2004; Birkeland & Brevik 2007; Haisch & Moddel 2008). Cole and Puthoff (1993) argue that ZP energy transfer for a class of extraction methods is not in violation of thermodynamic laws.

To understand the possibilities, a stack consisting of alternating tunably conductive and piezo layers bounded by conducting electrodes is envisaged, as illustrated in Figure 1. The ZP compression of the piezo

produces both a mechanical spring-like potential, which drives its elastic separation when the ZP force is turned off, and an electrical potential, which can provide some energy to an external circuit. Though models of the Casimir force usually suppose infinitely thick sandwiching plates, the determining ZP fluctuations are in the conducting surfaces, with solutions little changed even with plates as thin as their separations.

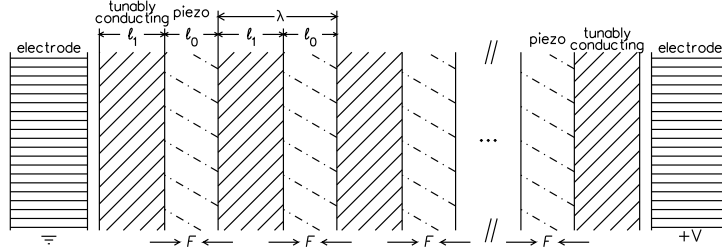


Figure 1: Stack of alternating tunably conductive and piezo plates. Switching the tunably conductive plates to conduct and then insulate produces a Casimir ZP compression of the intermediate piezos followed by their elastic reexpansion, giving a net work from which useful electrical energy might be derived.

The modulation of the Casimir effect by the conductive cycling of semiconductors with laser light has been demonstrated in precise differential tests, which validate theoretical estimates to within 1% (Caride et al. 2005; Klimchitskaya et al. 2009). Novel semiconductor conductivity switching schemes are described in the literature (Lipkin 1996). Semiconductor modulation at rates up to about $\nu = 10$ THz by electrical modulation in adjacent oppositely doped layers for modern transistor design has been demonstrated (Cooke 2007), and deposited layers only 5 nm thick, about 18 atoms, are reached in microlayer nanotechnology, like what is used in integrated circuits. With such rates and scales, the maximum possible ZP power that might be made available with an ideal perfect conductor in alternating layers is in the range of 60 kW/cm^3 of the stack volume, but drops off very rapidly using realistic material conductors or semiconductors to $<120 \text{ W/cm}^3$, as elaborated in Appendix A. Though a possibly viable arrangement, this paper considers the alternating-layer stack only as a conceptual example to help understand qualitatively similar, but more natural forms of ZP force modulation with better possibilities for much more appreciable energy extraction.

Here the ZP dynamics of acoustic waves is considered. A plane pressure wave produces a 1D periodic graded index-of-refraction or permittivity variation by the acousto-optic effect, giving parallel planes of alternating permittivity through a medium, as illustrated in Figure 2. A permittivity variation is a generalized form of conductivity variation, so neighboring plane wave crests (or troughs) should exhibit a ZP force between them, like alternating discrete conducting plates in a stack, giving longitudinal pressure variations within the medium, as illustrated by the ZP force vectors F .

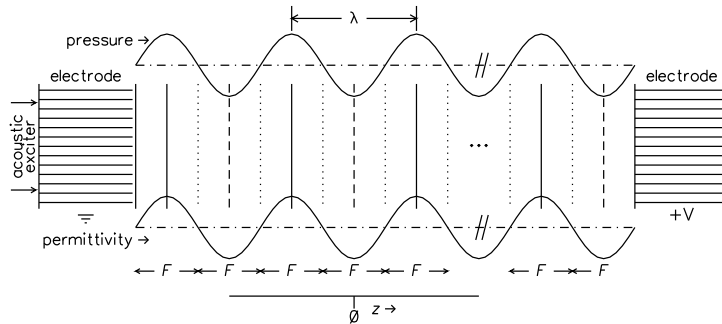


Figure 2: ZP forces in an acoustic wave. Neighboring permittivity plane wave crests (or troughs) produced in an acoustic wave should interact like alternating discrete parallel layers to give ZP pressures within the medium.

It appears that ZP forces in acoustic waves have not been discussed before in the scientific literature, yet it is predicted that effects can be large. The ‘acoustic Casimir effect’ is an analogue for the Casimir effect wherein acoustic waves play the role of the background ZP fluctuating field. Acoustic waves, like ZP fluctuations, behave like ocean waves outside nearby ships, which force them together as their hulls impose destructive interference on the waves between them, an effect known to ancient mariners for its potentially hazardous consequences.

ZP forces in graded-permittivity media have been considered mainly to understand the effects of soft boundaries on three-layer solutions, and unlike discrete layers, are described by divergent quantum integrals, which may suggest an enhanced effect (Inui 2003; Podgornik & Parsegian 2004; Philbin et al. 2010). The ZP force in a material with a 1D spatially varying permittivity is formulated in Section 2, with Fourier-series solutions derived in Section 3 using an appropriate high-frequency cutoff to avoid quantum integral divergences, and with numerical examples for a permittivity wave presented in Section 4. The ZP force in a periodic waveform of graded permittivity is indeed found to be greatly enhanced in amplitude compared to the Casimir ZP force in the otherwise equivalent stack of discrete layers for spatial repetition scales even as small as atomic dimensions. It extends to larger repetition scale λ decreasing only as $1/\lambda^2$, exhibits no temperature sensitivity, and is repulsive in a sinusoidal wave.

A permittivity wave produces mainly two ZP harmonics: of bulk dc and double wavenumber. As a standing acoustic wave is cycled in time, the ZP force turns on and off. The same sign of ZP bulk force occurs at both wave extremes, but vanishes as the standing wave passes through its null, giving a body force modulated at twice the acoustic wave frequency, as illustrated in the timeline in Figure 3. But such repeated body tensing in a piezo crystal is a usual energy-harvesting scenario, suggesting that ZP energy might be derived from a standing acoustic wave through end electrodes in a ‘crystal power’ optical arrangement like that illustrated in Figure 2. In a traveling acoustic wave, no ZP energy transfer occurs as the ZP bulk harmonic is not modulated.

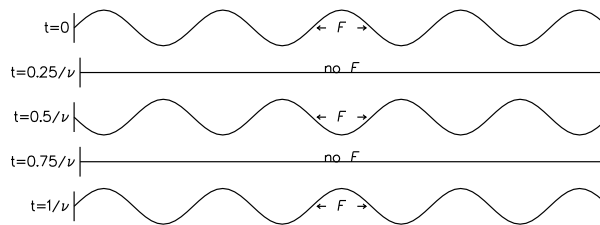


Figure 3: Cycling of ZP pressure in a standing acoustic wave of frequency ν cycles per sec in time t . The ZP bulk repulsive (expansive) force in a standing permittivity wave is modulated at twice the acoustic wave frequency.

The ZP bulk repulsive force in a standing acoustic wave may be represented as a traction force acting within the volume of the piezo crystal, which produces both stress and strain mechanical variations as discussed in Section 5. The piezo effect introduces a shift in the temporal phase between the mechanical stress and strain cycles and correspondingly between the electric-field and electric-displacement cycles, representing a transfer of energy in a conservative system. The energetic coupling of the mechanical cycle to an external electrical load (or supply), shifts the stress cycle in phase to lead (or lag) the strain, producing a single-signed cycling electric displacement that leads (or lags) a single-signed oscillating electric field, which represents a systematic transfer of energy out of (or into) the mechanical cycle, driven by (or in opposition to) ZP forces.

As the ZP bulk pressure produces a single-signed piezo voltage across the crystal volume, even the out-of-phase modulation in finite domains should add to give a net voltage effect. Possibilities for the excitation of standing acoustic waves in piezo crystals relevant for a voltage effect are discussed in Section 6.

2 1D ZP Force

ZP forces arise in a medium with a 1D spatial z permittivity variation $\varepsilon[\xi, z]$ as in an alternating-layer stack like that illustrated in Figure 1, or in an acoustic wave in Figures 2 and 3. The general complex permittivity $\varepsilon[\xi, z]$ characterizes fully the electro-optic properties of a medium, defining its retardation and absorption as a function of light frequency ξ . The ZP force is derived in many places especially after the Lifshitz collaboration (Lifshitz 1956; Dzyaloshinskii et al. 1961; see Milonni 1994, Chapter 7), and measurements like those described in the introduction, validate their solution in retarding and absorbing media. The ZP force per unit area (or pressure) with positive as expansive is written as a function of position z

$$F[z] = -\frac{k_B \Theta}{\pi c^2} \sum_{m=0}^{\infty} \left(\frac{1}{2}\right)^{(m==0)} \int_0^{\infty} \kappa[z] (\mathcal{R}_s[z] + \mathcal{R}_p[z]) \omega d\omega, \quad (1)$$

for k_B Boltzmann's constant and Θ the temperature. The sum over m counts the Matsubara mode frequencies $\xi = m2\pi k_B \Theta / \hbar = m(\Theta/300\text{K}) \cdot 2.47\text{E}14$ rad/s, which enter implicitly under the integral; as usual $\hbar = 2\pi\hbar$ is Planck's constant and c the speed of light. The logical function is used with $(m==0) = 1$ on true or 0 on false, giving an $m = 0$ summation term that receives half weight. For ease in reading the complicated relations, square braces are used throughout this paper to denote functional dependencies.

The reflection terms for perpendicular (senkrecht) s and parallel p ZP polarized rays are defined

$$\mathcal{R}_{\tilde{s}}[z] = \frac{R_{\tilde{s}+}[z]R_{\tilde{s}-}[z]}{1 - R_{\tilde{s}+}[z]R_{\tilde{s}-}[z]}, \quad (2)$$

for Fresnel reflection coefficients $R_{\tilde{s}\pm}[z]$, which depend upon the spatial position z as well as the permittivity. The wavenumber $\kappa[z]$ for the ZP evanescent electromagnetic modes is defined by the mode frequencies ξ and ω

$$\kappa[z] = \frac{1}{c} (\tilde{\varepsilon}[\xi, z]\xi^2 + \omega^2)^{\frac{1}{2}}. \quad (3)$$

The definitions for the real wavenumber $\kappa[z]$ and Fresnel reflection coefficients $R_{\tilde{s}\pm}[z]$ are based upon the real permittivity $\tilde{\varepsilon}[\xi, z] \equiv \varepsilon[i\xi, z]$, the projection of the general complex permittivity on its imaginary frequency axis, which casts the complex $\varepsilon[i\xi]$ into a real function $\tilde{\varepsilon}[\xi]$ of real frequency ξ consistent with the Kramers-Krönig causality constraints (Hough & White 1980; see Appendix A). Fresnel reflection coefficients for evanescent waves defined using the real projected permittivity $\tilde{\varepsilon}_j[\xi]$ give a convenient real solution form for mixed retarding and absorbing multilayers. Variables retain dependencies on frequencies implicitly as a dependence on ξ in the permittivity $\tilde{\varepsilon}[z]$, and dependencies on ξ and ω in the wavenumber $\kappa[z]$.

It is usual to replace the sum over Matsubara frequencies in (1) by an integral. Symbolically the sum is approximated $\sum_{m=0}^{\infty} (1/2)^{(m==0)} \dots \rightarrow \int_0^{\infty} \dots dm$, which takes properly into account the half-size interval at the lower $m = 0$ limit. Substituting for the sum in this way, and using the interval $dm = (\hbar/(2\pi k_B \Theta))d\xi$ from the definition for the Matsubara frequency ξ , gives the integral for the ZP force

$$F[z] = -\frac{\hbar}{2\pi^2 c^2} \int_0^{\infty} \int_0^{\infty} \kappa[z] (\mathcal{R}_s[z] + \mathcal{R}_p[z]) \omega d\omega d\xi, \quad (4)$$

which is independent of temperature Θ , and so represents the zero-temperature $\Theta = 0\text{K}$ solution.

Simply substituting an integral for the sum is a good approximation when the main contribution to the sum comes from terms with $m \gg 1$. Thus temperature effects are only important when terms of low frequency ξ or small wavenumber κ are significant in sum, which occurs when the layer thickness ℓ is comparable to or greater than the light wavelength for the Matsubara base frequency $\ell \gtrsim c/\xi[m=1] = c/(2\pi k_B \Theta / \hbar) = (300\text{K}/\Theta) \cdot 1.2148\text{E}-4$ cm. As is illustrated in numerical examples in Figure 11 in Appendix A, temperature effects in multilayer solutions are indeed of vanishing importance when the middle-layer thickness is less than about $\text{E}-4$ cm = $1 \mu\text{m}$. The summation for finite temperature effects can be considered via Abel-Plana formulae (Dowling 1989).

The Lifshitz collaborative QED formulation given in Dzyaloshinskii et al. (1961) has been shown to be applicable in a 1D stack with an arbitrary number of multilayers (Ninham & Parsegian 1970; Podgornik et al. 2003). Fresnel reflection coefficients are propagated in $+z$ by recursion as $R_{\bar{s}+}[z]$ from $z = -\infty$ or in $-z$ as $R_{\bar{s}-}[z]$ from $z = +\infty$ following the comprehensive formula for evanescent waves (Jacobsson 1965; Zhou & Spruch 1995; Born & Wolf 1980, Section 1.6). The $+z$ propagated reflection coefficient changes from $R_{\bar{s}+}[<z_j]$ just below the permittivity jump at z_j up to the next following jump at z_{j+1} as

$$R_{\bar{s}+}[z_j < z < z_{j+1}] = \frac{R_{\bar{s}+}[<z_j] + r_{\bar{s}j}}{1 + R_{\bar{s}+}[<z_j]r_{\bar{s}j}} e^{-2\kappa_j(z-z_j)}, \quad (5)$$

using $R_{\bar{s}+}[<z_j]$ to denote the value of $R_{\bar{s}+}$ preceding or smoothly asymptotic with $z = z_j$ from below. The interfacial reflections are defined

$$r_{sj} = \frac{\kappa_{j-1} - \kappa_j}{\kappa_{j-1} + \kappa_j}, \quad r_{pj} = \frac{\check{\epsilon}_j \kappa_{j-1} - \check{\epsilon}_{j-1} \kappa_j}{\check{\epsilon}_j \kappa_{j-1} + \check{\epsilon}_{j-1} \kappa_j}, \quad (6)$$

for permittivities $\check{\epsilon}_j$ and wavenumbers κ_j in layers numbered j , with ℓ_j the layer thickness as illustrated in Figure 4. In a stack with equal layer thicknesses $\ell_j = \ell$, the jumps are located at $z_j = (j - \frac{1}{2})\ell$, $z_{-1} = -\frac{3\ell}{2}$, $z_0 = -\frac{\ell}{2}$, $z_1 = \frac{\ell}{2}$, $z_2 = \frac{3\ell}{2}$, etc. Alternating-layer arrangements are considered too, which have two thicknesses with $\ell_j = \ell_0$ in even j layers and $\ell_j = \ell_1$ in odd j layers.

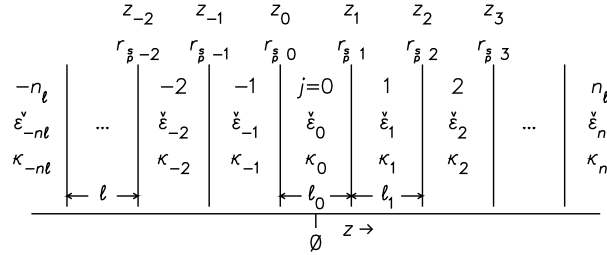


Figure 4: Plane-parallel $2n_\ell + 1$ multilayer stack consisting of projected permittivities $\check{\epsilon}_j$ and wavenumbers κ_j in layers j counted from a middle layer $j = 0$, with interfacial reflections r_{sj} and r_{pj} at the jumps z_j between layers.

Similarly the $-z$ propagated reflection coefficient changes from $R_{\bar{s}-}[>z_{j+1}]$ succeeding or just above the boundary between layers $j + 1$ to j , to smaller z down to the next boundary at z_j , with the formula

$$R_{\bar{s}-}[z_{j+1} > z > z_j] = \frac{R_{\bar{s}-}[>z_{j+1}] - r_{\bar{s}(j+1)}}{1 - R_{\bar{s}-}[>z_{j+1}]r_{\bar{s}(j+1)}} e^{-2\kappa_j(z_{j+1}-z)}, \quad (7)$$

with the interfacial reflections across the jump defined in (6), noting reversed signs for the reversed propagation direction in z compared to Eq. (5).

The Fresnel reflection coefficients decrease exponentially in $+z$ from $R_{\bar{s}+}[>\frac{-\ell_0}{2}] = (R_{\bar{s}+}[<\frac{-\ell_0}{2}] + r_{\bar{s}0})/(1 + R_{\bar{s}+}[<\frac{-\ell_0}{2}]r_{\bar{s}0})$ just above the $z_0 = \frac{-\ell_0}{2}$ jump in Eq. (5), and in $-z$ from $R_{\bar{s}-}[<\frac{\ell_0}{2}] = (R_{\bar{s}-}[>\frac{\ell_0}{2}] - r_{\bar{s}1})/(1 - R_{\bar{s}-}[>\frac{\ell_0}{2}]r_{\bar{s}1})$ just below the $z_1 = \frac{\ell_0}{2}$ jump in Eq. (7). They vary across the middle layer $\frac{-\ell_0}{2} < z < \frac{\ell_0}{2}$ as

$$R_{\bar{s}+}[z] = R_{\bar{s}+}[>\frac{-\ell_0}{2}]e^{-2\kappa_0(z+\frac{\ell_0}{2})}, \quad R_{\bar{s}-}[z] = R_{\bar{s}-}[<\frac{\ell_0}{2}]e^{-2\kappa_0(\frac{\ell_0}{2}-z)},$$

and in their product, the z dependence vanishes

$$R_{\bar{s}+}[z]R_{\bar{s}-}[z] = R_{\bar{s}+}[>\frac{-\ell_0}{2}]R_{\bar{s}-}[<\frac{\ell_0}{2}]e^{-2\kappa_0\ell_0}, \quad (8)$$

giving $\mathcal{R}_{\tilde{p}}$ from (2) and a Casimir force F from (1) or (4) independent of z across a constant permittivity layer within jumps on either side. A constant ZP force across a uniform layer is a well-known property of ZP force solutions.

A three-layer stack has the Fresnel reflection coefficient $R_{\tilde{p}+}[\succ \frac{-\ell_0}{2}] = r_{\tilde{p}0}$ above its lower jump at $z = \frac{-\ell_0}{2}$, projecting with Eq. (5) from a uniform media everywhere below $R_{\tilde{p}+}[z < \frac{-\ell_0}{2}] = 0$. It has the reflection coefficient $R_{\tilde{p}-}[\prec \frac{\ell_0}{2}] = -r_{\tilde{p}1}$ below its upper jump at $z = \frac{\ell_0}{2}$, projecting with (7) from a uniform media everywhere above $R_{\tilde{p}-}[z > \frac{\ell_0}{2}] = 0$. Combining gives the product $R_{\tilde{p}+}[z]R_{\tilde{p}-}[z] = -r_{\tilde{p}0}r_{\tilde{p}1} \exp[-2\kappa_0\ell_0]$ in the middle layer $\frac{-\ell_0}{2} < z < \frac{\ell_0}{2}$ from (8). With (6), the product leads to the Lifshitz collaborative formula (Dzyaloshinskii et al. 1961, Eq. (4.14)).

A five-layer stack $n_\ell = 2$ with layers of equal thicknesses ℓ counted $-2 \leq j \leq 2$ has four contained jumps, at $z_{-1} = \frac{-3\ell}{2}$, $z_0 = \frac{-\ell}{2}$, $z_1 = \frac{\ell}{2}$, and $z_2 = \frac{3\ell}{2}$ as in Figure 4. The Fresnel reflection coefficient in (8) comes from the $+z$ propagated coefficient just above the jump at z_{-1} , $R_{\tilde{p}+}[\succ \frac{-3\ell}{2}] = r_{\tilde{p}-1}$, which gives $R_{\tilde{p}+}[\prec \frac{-\ell}{2}] = r_{\tilde{p}-1} \exp[-2\kappa_{-1}\ell]$ just below the next jump at z_0 , and then the needed $R_{\tilde{p}+}[\succ \frac{-\ell}{2}]$ across z_0 with $r_{\tilde{p}0}$ using Eq. (5). Similarly the Fresnel reflection coefficient just below the jump at z_2 , $R_{\tilde{p}-}[\prec \frac{3\ell}{2}] = -r_{\tilde{p}2}$, is propagated in $-z$ to yield $R_{\tilde{p}-}[\succ \frac{\ell}{2}] = -r_{\tilde{p}2} \exp[-2\kappa_1\ell]$ just above the next lower jump at z_1 , and then the needed $R_{\tilde{p}-}[\prec \frac{\ell}{2}]$ below z_1 with $r_{\tilde{p}1}$ using Eq. (7). The resulting product of reflection coefficients in Eq. (8) agrees with Zhou and Spruch (1995, Eqs. (3.12)–(3.16)).

Though changing symbols and formulae add serious complications, the Casimir force in (1) or (4) with any number of layers appears to be consistent with what is developed and discussed in numerous studies (Tomaš 2002; Raabe et al. 2003; Henkel & Joulain 2005; Ellingsen 2007).

A sandwich of two identical layers around a middle layer $j = 0$ with permittivities $\tilde{\epsilon}_1 = \tilde{\epsilon}_{-1}$ has jump coefficients $r_{\tilde{p}0} = -r_{\tilde{p}1}$, and so a product of reflection coefficients $R_{\tilde{p}+}[z]R_{\tilde{p}-}[z] = r_{\tilde{p}0}^2 \exp[-2\kappa_0\ell_0] > 0$ or $\mathcal{R}_{\tilde{p}}[z] > 0$ from (2), meaning that the Casimir ZP force $F[z]$ defined in Eqs. (1) or (4) is negative or attractive. It can be seen too that recursive application of the formulae (5) and (7) in a spatially symmetric arrangement around a middle layer $j = 0$ with $\tilde{\epsilon}_j = \tilde{\epsilon}_{-j}$, for any number of layers even of varying thicknesses with $\ell_j = \ell_{-j}$, gives $R_{\tilde{p}+}[\succ \frac{-\ell_0}{2}] = R_{\tilde{p}-}[\prec \frac{\ell_0}{2}]$, and so in the middle layer $R_{\tilde{p}+}[z]R_{\tilde{p}-}[z] > 0$, $\mathcal{R}_{\tilde{p}}[z] > 0$, and an attractive ZP force $F[z] < 0$ (as in Lambrecht et al. 1997; Henkel & Joulain 2005). For a symmetric arrangement it also follows that $R_{\tilde{p}+}[z] = R_{\tilde{p}-}[-z]$ or $R_{\tilde{p}+}[z]R_{\tilde{p}-}[z] = R_{\tilde{p}+}[-z]R_{\tilde{p}-}[-z]$, giving $\mathcal{R}_{\tilde{p}}[z] = \mathcal{R}_{\tilde{p}}[-z]$, and so a symmetric ZP force $F[z] = F[-z]$ for all z .

In principle the ω integral in Eqs. (1) and (4) may be divergent, as the interfacial reflections r_{pj} from (6) do not vanish as $\omega \rightarrow \infty$, and these enter into the reflection coefficients $R_{p\pm}[z]$ and reflection term \mathcal{R}_p . However the attenuation factor $\exp[-2\kappa_0\ell_0]$, which multiplies the product of the reflection coefficients from the two nearest jumps in (8), does go to zero as ω goes to infinity for finite ℓ_0 , since κ_0 from Eq. (3) increases with ω . Thus quantum divergences are not seen where the permittivity is constant across a finite layer.

For a three-layer stack, the ZP force integral Eq. (4) in a middle layer of thickness ℓ_0 is conveniently rewritten in terms of a new dimensionless integration variable $\eta = \kappa_0\ell_0 = (\tilde{\epsilon}[\xi]\xi^2 + \omega^2)^{1/2}\ell_0/c$, which substitutes for the frequency ω . Using the derivative $\partial\eta^2/\partial\omega^2 = (\ell_0/c)^2$ or $\eta d\eta = (\ell_0/c)^2\omega d\omega$, reforms the ω integral into an integral in η as

$$F = -\frac{\hbar}{2\pi^2\ell_0^3} \int_0^\infty \int_0^\infty \eta^2 (\mathcal{R}_s + \mathcal{R}_p) d\eta d\xi. \quad (9)$$

As described in Appendix B, for a small middle-layer thickness ℓ_0 , the η integrand is determined by the product $\eta^2 \exp[-2\eta]$, and the ZP force variation with ℓ_0 follows the external factor $1/\ell_0^3$. The product $\eta^2 \exp[-2\eta]$ has its maximum around $\eta = 1$, corresponding to the wavenumber $\kappa_0 = 1/\ell_0$, and drops off exponentially beyond.

Other limiting forms arise when the middle-layer thickness is greater than a cross-over scale $\ell_0 > \ell_\pm$, as most usually a $1/\ell_0^4$ ZP force retarded dependence as elaborated in Appendices A and B. Symmetric multilayer stacks exhibit the same asymptotic behavior as a three-layer stack, since ZP forces are determined in the nearest layers.

3 In a Graded Permittivity

The definition for the ZP force from Eq. (1) should be applicable too in a stratified medium with a 1D smoothly varying complex permittivity $\varepsilon[z]$ or real $\tilde{\varepsilon}[z]$ and corresponding real $\kappa[z]$ defined by Eq. (3). In the limit that the layer thickness ℓ becomes infinitesimal, the Fresnel recursion formulae Eqs. (5) and (7) produce differential equations for a graded permittivity.

The expression for the reflection coefficient at the high z end of the $j = 0$ interval $R_{\tilde{p}\pm}[\prec\frac{\ell}{2}]$ in terms of its value just below the low z jump $R_{\tilde{p}\pm}[\prec\frac{\ell}{2}]$ from Eq. (5), with the substitution of Taylor series' in powers of ℓ , $R_{\tilde{p}\pm}[\prec\pm\frac{\ell}{2}] = R_{\tilde{p}\pm}[0] \pm (\partial R_{\tilde{p}\pm}/\partial z)\frac{\ell}{2} + \dots$, $r_{\tilde{p}0} = \rho_{\tilde{p}}[-\frac{\ell}{2}]\ell = \rho_{\tilde{p}}[0]\ell - (\partial\rho_{\tilde{p}}/\partial z)\ell^2/2 + \dots$, and $\exp[-2\kappa_0\ell] = 1 - 2\kappa_0\ell + \dots$, gives the differential equation for $R_{\tilde{p}\pm}[z]$ around $z = 0$

$$\frac{\partial R_{\tilde{p}\pm}}{\partial z} = \rho_{\tilde{p}}[z](1 - R_{\tilde{p}\pm}[z]^2) \mp 2\kappa[z]R_{\tilde{p}\pm}[z], \quad (10)$$

introducing the smoothly varying reflection $\rho_{\tilde{p}}[z_j] \equiv r_{\tilde{p}j}/\ell$, and keeping terms only to lowest order in ℓ . The differential equation for $R_{\tilde{p}-}[z]$ is contained in this equation also, which is found similarly by defining the reflection coefficient for the low z end of the $j = 0$ interval $R_{\tilde{p}-}[\succ\frac{\ell}{2}]$ in terms of its value just above the high z jump $R_{\tilde{p}-}[\succ\frac{\ell}{2}]$ using Eq. (7), with the additional Taylor series' $R_{\tilde{p}-}[\succ\pm\frac{\ell}{2}] = R_{\tilde{p}-}[0] \pm (\partial R_{\tilde{p}-}/\partial z)\frac{\ell}{2} + \dots$, and $r_{\tilde{p}1} = \rho_{\tilde{p}}[\frac{\ell}{2}]\ell = \rho_{\tilde{p}}[0]\ell + (\partial\rho_{\tilde{p}}/\partial z)\ell^2/2 + \dots$. Though relations are derived for around $z = 0$, they are applicable at all z in the small ℓ limit for an infinite multilayer stack.

The smoothly varying reflection $\rho_{\tilde{p}}[z_j] \equiv r_{\tilde{p}j}/\ell$ is introduced as it remains well defined in the small ℓ limit. The wavenumber and permittivity first derivatives are taken to be the jump differences between layers normalized by the layer thickness ℓ , as $\partial\kappa/\partial z = (\kappa_0 - \kappa_{-1})/\ell$ and $\partial\tilde{\varepsilon}/\partial z = (\tilde{\varepsilon}_0 - \tilde{\varepsilon}_{-1})/\ell$. Substituting into Eq. (6) with the values at $z = 0$, $\kappa[0] = \kappa_0$ and $\tilde{\varepsilon}[0] = \tilde{\varepsilon}_0$, then yields around $z = 0$

$$\begin{aligned} \rho_s[z] &= -\frac{1}{2\kappa[z]} \frac{\partial\kappa}{\partial z} = -\left(\frac{\xi}{2c\kappa[z]}\right)^2 \frac{\partial\tilde{\varepsilon}}{\partial z}, \\ \rho_p[z] &= \frac{1}{2\tilde{\varepsilon}[z]} \frac{\partial\tilde{\varepsilon}}{\partial z} - \frac{1}{2\kappa[z]} \frac{\partial\kappa}{\partial z} = \left(\frac{1}{2\tilde{\varepsilon}[z]} - \left(\frac{\xi}{2c\kappa[z]}\right)^2\right) \frac{\partial\tilde{\varepsilon}}{\partial z}, \end{aligned} \quad (11)$$

written for $\ell \rightarrow 0$, and again recognizing that the relations remain applicable at all z in an infinite multilayer stack. The differential Eq. (10) with (11) agrees with evanescent solutions from different formulations for the propagation of waves in a stratified medium (e.g. see Jacobsson 1965, Eq. (2.37); Lekner 2016, Chapter 5; and references).

For everywhere-small reflection coefficients $|R_{\tilde{p}\pm}[z]| \ll 1$, consistent with small-amplitude periodic permittivity variations on top of a constant permittivity background, Eq. (10) can be linearized, which provides the closed-form integral solution

$$R_{\tilde{p}\pm}[z] = e^{\mp 2 \int \kappa[z] dz} \int e^{\pm 2 \int \kappa[z] dz} \rho_{\tilde{p}}[z] \left(1 - \tilde{R}_{\tilde{p}\pm}[z]^2\right) dz, \quad (12)$$

where the function $\tilde{R}_{\tilde{p}\pm}[z]$ represents a prior approximation to the propagated Fresnel reflection coefficient.

ZP forces in a medium of graded permittivity are studied by Fourier analysis supposing relatively small reflection coefficients, which gives a denominator near one in $\mathcal{R}_{\tilde{p}}[z]$ from (2), and a ZP force from (4) well approximated as

$$F[z] = -\frac{\hbar}{2\pi^2 c^2} \int_0^\infty \int_0^\infty \kappa[z] (R_{s+}[z]R_{s-}[z] + R_{p+}[z]R_{p-}[z]) \omega d\omega d\xi. \quad (13)$$

The approximations used here are quantified in numerical calculations described in Section 4.

The Fourier transform of a repeating spatial profile of some repetition length λ can be expanded in a discrete Fourier series in wavenumbers n/λ cycles per cm for integer modes n , extending in principle from

$-\infty < n < \infty$, written for the ZP force as

$$F[z] = \sum_n \bar{F}_n e^{i2\pi n \frac{z}{\lambda}}, \quad (14)$$

in Fourier modes \bar{F}_n , or similarly for the reflection coefficients $R_{\bar{p}\pm}[z]$ in modes $\bar{R}_{(\bar{p}\pm)n}$, or for the smoothly varying reflections $\rho_{\bar{p}}[z]$ in modes $\bar{\rho}_{\bar{p}n}$. The Fourier modes are Hermitian with $\bar{F}_{-n} = \bar{F}_n^*$ for a real function $F[z]$, or are real with $\bar{F}_{-n} = \bar{F}_n$ for a symmetric function around $z = 0$, $F[z] = F[-z]$.

Substituting Fourier series' for the variables transforms the differential Eq. (10) into the algebraic equation in Fourier modes

$$\bar{R}_{(\bar{p}\pm)n} = \frac{\bar{\rho}_{\bar{p}n}}{\pm 2\kappa + i2\pi n/\lambda}, \quad (15)$$

ignoring the square of the reflection coefficient, and spatial variations in the wavenumber κ . Solutions for the ZP force are found with κ in Eq. (3) determined by a diverging frequency ω , which is spatially constant.

With κ greater than the largest significant wavenumbers n/λ in the smoothly varying reflection, Eq. (15) gives the proportionality $\bar{R}_{(\bar{p}\pm)n} \sim \bar{\rho}_{\bar{p}n}/\kappa$ in every important Fourier mode n , which means spatial quantities similarly go as $R_{\bar{p}\pm} \sim \rho_{\bar{p}}/\kappa$, and the product of reflection coefficients as $R_{\bar{p}+}R_{\bar{p}-} \sim \rho_{\bar{p}}^2/\kappa^2$. From Eq. (11), $\rho_s \sim 1/\kappa^2$, and the product of reflection coefficients goes as $R_{s+}R_{s-} \sim 1/\kappa^6$. On the other hand, the first term in the smoothly varying reflection ρ_p from Eq. (11) is independent of κ , which gives $R_{p+}R_{p-} \sim 1/\kappa^2$ asymptotically for large κ . All in all, the first term in ρ_p leads to a linearly divergent ω integral in Eq. (13), whereas integrals of the other cross-product terms and of the product $R_{s+}R_{s-}$ are convergent, and can be ignored by comparison. Thus only the first term in the parallel smoothly varying reflection determines the ZP force

$$\rho_p[z] = \frac{1}{2} \frac{\partial \ln[\tilde{\epsilon}]}{\partial z}. \quad (16)$$

So, with a smoothly varying permittivity, the integral over ω in (13) is indeed divergent and feels its maximum contribution from frequencies ω approaching a cutoff ω_x . On the other hand, the Matsubara frequency ξ has a limited range of significant contribution as the spatial derivative of the permittivity $\tilde{\epsilon}$, and so the smoothly varying reflection $\rho_p[z]$ in Eq. (16), disappear well below any physically reasonable cutoff with $\xi \ll \omega_x$, and with them the reflection coefficient $R_{p\pm}$ from the Fourier relation Eq. (15). Thus the wavenumber in (3) is well approximated as $\kappa = \omega/c$. This result is quite unlike what was found with a constant permittivity in a finite layer ℓ where the ZP force integral (9) has its maximum contribution around the relatively small wavenumber $\kappa = 1/\ell$.

Expressing the permittivity as a Fourier series' too, but in its logarithm

$$\ln[\tilde{\epsilon}[z]] = \sum_n \overline{\{\ln \tilde{\epsilon}\}}_n e^{i2\pi n \frac{z}{\lambda}}, \quad (17)$$

for complex coefficients $\overline{\{\ln \tilde{\epsilon}\}}_n$, yields for the smoothly varying reflection from Eq. (16), and for the reflection coefficient from (15)

$$\bar{\rho}_{pn} = \frac{i\pi n}{\lambda} \overline{\{\ln \tilde{\epsilon}\}}_n, \quad \bar{R}_{(p\pm)n} = \frac{1}{2} \frac{in}{\pm \frac{\omega\lambda}{\pi c} + in} \overline{\{\ln \tilde{\epsilon}\}}_n, \quad (18)$$

using $\kappa = \omega/c$. Substituting into the ZP force integral Eq. (13) with $R_{s\pm} = 0$ and the Fourier series' for the reflection coefficient $R_{p\pm}[z]$ in its modes $\bar{R}_{(p\pm)n}$ from Eq. (18), then gives a Fourier series for the ZP pressure Eq. (14) with the mode coefficients

$$\bar{F}_n = \frac{\hbar}{8\pi^2 c^3} \sum_q \int_0^\infty (n-q)q \overline{\{\ln \tilde{\epsilon}\}}_{n-q} \overline{\{\ln \tilde{\epsilon}\}}_q d\xi \int_0^\infty \frac{\omega^2}{\left(\frac{\omega\lambda}{\pi c} + in - iq\right) \left(\frac{\omega\lambda}{\pi c} + iq\right) \left(1 + \left(\frac{\omega}{\omega_x}\right)^2\right)^2} d\omega. \quad (19)$$

where the sum over \pm integers q represents a convolution, which arises with the product of Fourier series'. The ω integral has a smooth Lorentzian cutoff around an upper limit ω_x introduced with the inserted term

in divisor $(1 + (\omega/\omega_x)^2)^2$, which imposes a form of covariant regularization (Feynman & Hibbs 1965, Section 9.6, after Eq. (9-89); Mandl & Shaw 2010, Section 9.2, Eq. (9.9)). The light wavelength for the cutoff is correspondingly $\lambda_x = 2\pi c/\omega_x$.

All explicit dependencies upon the repetition scale λ factor out of the ω integral, substituting for ω with a dimensionless $\hat{\omega} = \omega\lambda_x/(\pi c)$, and for n and q with the scaled-down $\hat{n} = n\lambda_x/\lambda$ and $\hat{q} = q\lambda_x/\lambda$. The frequency ratio has the equivalences $\omega/\omega_x = \lambda_x/\lambda = \hat{\omega}/\hat{\omega}_x$, where $\hat{\omega}_x = \omega_x\lambda_x/(\pi c) = 2$. With some rearranging, the ZP force mode becomes

$$\bar{F}_n = -\frac{\pi^2\hbar}{16\lambda_x\lambda^2} \sum_q (n-q)q \mathfrak{C} \int_0^\infty \overline{\{\ln \tilde{\varepsilon}\}}_{n-q} \overline{\{\ln \tilde{\varepsilon}\}}_q d\xi, \quad (20)$$

with

$$\mathfrak{C} = \frac{32}{\pi} \int_0^\infty \frac{\hat{\omega}^2}{(\hat{\omega} - i\hat{n} + i\hat{q})(\hat{\omega} + i\hat{q})(\hat{\omega} - 2i)^2(\hat{\omega} + 2i)^2} d\hat{\omega}. \quad (21)$$

The Fourier modes of the physical (real) quantities are Hermitian, $\bar{F}_{-n} = \bar{F}_n^*$ and $\overline{\{\ln \tilde{\varepsilon}\}}_{-n} = \overline{\{\ln \tilde{\varepsilon}\}}_n^*$, but the cutoff function \mathfrak{C} is real, and does not change by taking the complex conjugate of Eq. (20), and so must remain unchanged with the equivalent flipping of the signs of both n and q . It follows that the $\hat{\omega}$ frequency integrand in \mathfrak{C} must also be unchanged with the change of sign $\hat{\omega} \rightarrow -\hat{\omega}$, which gives for the integral $\int_{-\infty}^0 \dots d\hat{\omega} = \int_0^\infty \dots d\hat{\omega}$ as it appears in Eq. (21). The integral in the cutoff function is doubled as its domain is extended to span the full $\pm\hat{\omega}$ real axis. Looping over the upper (or equivalently lower) half complex $\hat{\omega}$ plane at infinity, which incurs no additional contribution, provides a contour in the continued $\hat{\omega}$ complex plane that encloses the $\hat{\omega} = 2i$ Cauchy residue plus contained or overlapping residues for $\hat{n} - \hat{q} > 0$ and $\hat{q} < 0$. A real resultant for \mathfrak{C} is found as shown in Figure 5, which ranges from 1 at the dc $\hat{n} - \hat{q} = \hat{q} = 0$, diminishes for larger wavenumbers, and becomes slightly negative for $(\hat{n} - \hat{q})\hat{q} \lesssim -2$ beyond the zero contour (dotted). The resulting cutoff function \mathfrak{C} is indeed symmetric with the simultaneous change of sign in n and q .

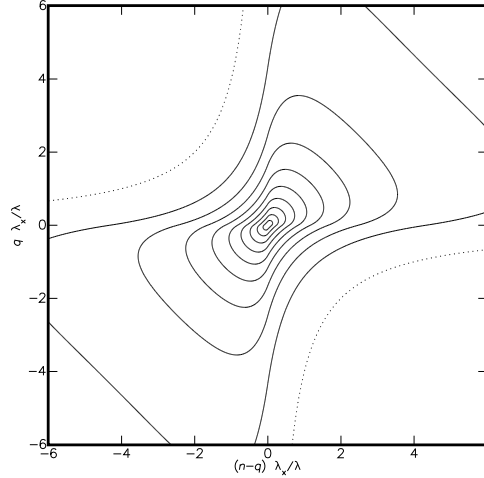


Figure 5: ZP force cutoff function \mathfrak{C} in wavenumber space ($\hat{n} = n\lambda_x/\lambda$, $\hat{q} = q\lambda_x/\lambda$) ranging from 1 at its maximum $n = q = 0$ to slightly negative outside the zero contour (dotted) with the contour interval 0.1.

The Fourier modes $\overline{\{\ln \tilde{\varepsilon}\}}_n$ for a given repeating waveform are independent of the wavelength λ , and so not changed with its rescaling. As long as the significant scales of variation in $\tilde{\varepsilon}[z]$ are large compared to the cutoff light wavelength $\lambda/n \gg \lambda_x$, the integral can be treated as a constant $\mathfrak{C} = 1$, giving a ZP force that decreases universally as the inverse square of the wavelength $1/\lambda^2$, from the external factor in Eq. (20). This ZP force property is validated in the numerical calculations for permittivity waves described in Section 4.

Even nonperiodic functional forms might be treated similarly approximated by discrete Fourier series', like multiple discrete interacting shaped structures of varying separation. However an effectively changing Fourier profile with separation distance for structures of fixed cross section introduces some scale dependencies into the ZP force modes. Consideration of more general functions is outside the scope of the present analysis, which is mainly concerned with the properties of permittivity waves.

A high frequency cutoff is often used for divergent quantum integrals at extinction scales natural to the problem. Schwinger, DeRaad, and Milton (1978) introduce an atomic-scale cutoff in normally divergent integrals that arise in their formulation of the Casimir effect for interacting atoms, and reproduce reasonably well measured values of the surface tension and latent heat of vaporization in liquid He at 0K. Milonni and Lerner (1992) find that an atomic-scale cutoff is justified in microscopic atomic theories applying the Ewald-Oseen extinction theorem for interacting atoms.

Permittivity variations in acoustic waves are due to changes in electronic vibration or conductive electronic states, as elaborated in Appendix A, so a Compton-frequency cutoff seems appropriate for the problem $\omega_x = \omega_C = m_e c^2 / \hbar = 7.7634\text{E}20$ rad/s, and is used for the calculations described in this paper. A Compton-frequency cutoff has been successfully applied with other ZP effects in electronic states, historically and most famously with the Lamb shift by Hans Bethe (Bethe 1947; Mandl & Shaw 2010, Section 9.6.2). The same cutoff is found using a quantum regularization procedure in a medium with a smoothly varying permittivity (Podgornik & Parsegian 2004). QED calculations for electronic processes exhibit a small but finite correlation length corresponding to the Compton-scattering scale, which can be taken to arise due to the limited electron recoil from interactions with virtual photons by the small but finite electron inertia (Peskin & Schroeder 1995, Chapters 8-9; see also Cavalleri & Spavieri 1989).

Since permittivity variations in acoustic waves arise with electronic states, they should flatten out on a scale comparable to that of Compton electron-photon scattering since the material substance is actually represented by spatially discrete reradiating electronic oscillators. Where the permittivity is constant over a finite scale ℓ , reflection coefficients become exponentially attenuated in frequency with their product going as $\exp[-2\omega\ell/c]$ as in Eq. (8) for a wavenumber $\kappa = \omega/c$, relevant for high-frequency processes. The ZP force ω integral Eq. (13) is governed by the weighting factor $\omega^2 \exp[-2\omega\ell/c]$ near the high frequency cutoff, which peaks at $\omega = c/\ell$ and drops off exponentially beyond. With a scale for flattening somewhat less than the Compton scattering wavelength $\ell = \lambda_C/(2\pi)$, where $\lambda_C = h/(m_e c) = 2.4263\text{E}-10$ cm, the integral of the weighting factor $\omega^2 \exp[-2\omega\ell/c]$ out to $\omega \rightarrow \infty$ is close to the integral over ω^2 alone sharply cut off at the Compton frequency ω_C , or the integral over ω^2 with an imposed Lorentzian cutoff around ω_C out to $\omega \rightarrow \infty$. It is known that retardation or dispersion can lead to a natural inherent quantum regularization (Horsley & Philbin 2014).

4 In a Permittivity Wave

Figure 6 shows an example ZP pressure profile $F[z]$ over one wavelength λ in (a) due to a sinusoidal permittivity wave $\tilde{\epsilon}[z]$ of representative wavelength and contrast (illustrated on top). The ZP pressure profile ranges from near zero to a maximum positive value for expansive in the most slopping portions of the permittivity wave.

For a permittivity variation symmetric about $z = 0$, the Fourier modes $\{\overline{\ln \tilde{\epsilon}}\}_n$ and correspondingly \bar{F}_n are real with $\bar{F}_{-n} = \bar{F}_n$ in Eq. (20), giving the cosine series for $n \geq 0$ from Eq. (14)

$$F[z] = \sum_{n=0} 2^{(n!=0)} \bar{F}_n \cos[2\pi n z / \lambda], \quad (22)$$

with the logical $(n! = 0)$, which is 1 on true and 0 on false, for double weight on all but the DC mode. Though most of the power in the profile (a) is in the bulk \bar{F}_0 and $\lambda/2 \bar{F}_2$ modes, a small residual containing mainly the \bar{F}_1 and \bar{F}_3 modes remains, which appears when the main ZP modes \bar{F}_0 and \bar{F}_2 are subtracted in (b). The subtraction is formulated strictly as $F[z] - \bar{F}_0 - 2\bar{F}_2 \cos[4\pi z / \lambda]$, with \bar{F}_0 positive and \bar{F}_2 negative. The ZP force difference between normal and sign-reversed permittivity waves in (c) appears to be close to two times the residual in (b).

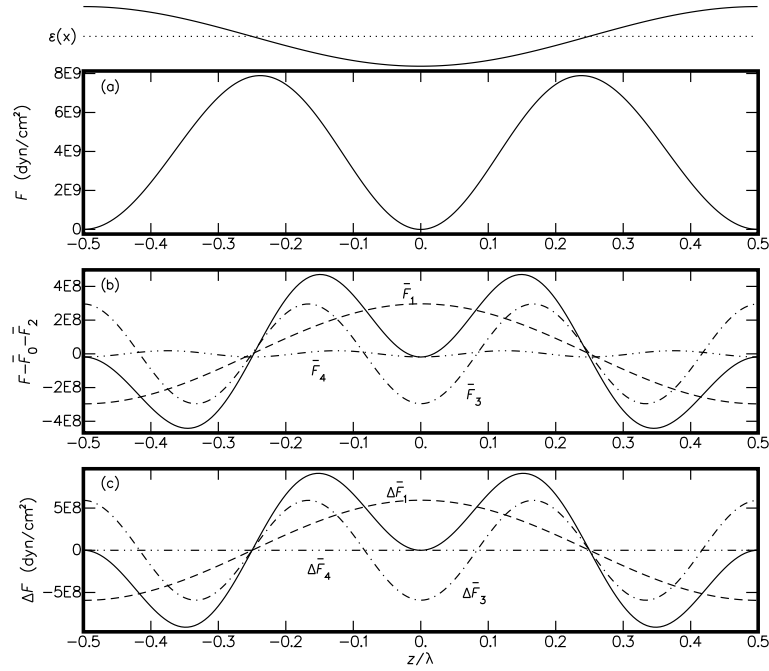


Figure 6: ZP pressure profile $F[z]$ in (a) for a sinusoidal permittivity wave (illustrated on top), with profiles for the main modes \bar{F}_0 and \bar{F}_2 subtracted in (b), and the ZP pressure difference profile $\Delta F[z]$ between the normal and sign-reversed permittivity waves in (c) (all solid), for wavelength $\lambda = \text{E}-6.5 \text{ cm} = 3.16 \text{ nm}$ and static-permittivity contrast $\Delta\epsilon_e/\langle\epsilon_e\rangle = 0.1$, and parameters characteristic of quartz. Profiles for component modes \bar{F}_1 , $\Delta\bar{F}_1$ (dashed), \bar{F}_3 , $\Delta\bar{F}_3$ (dot-dashed), \bar{F}_4 , and $\Delta\bar{F}_4$ (dot-dot-dashed) are also shown.

The ZP force model used for the figures is based on the Fourier decomposition from Section 3. The permittivity $\tilde{\epsilon}[z]$ is defined by Eqs. (33) and (34) in Appendix A with a sinusoidal wave in one parameter as static permittivity $\epsilon_e = \langle\epsilon_e\rangle + \Delta\epsilon_e \cos 2\pi z/\lambda$, and the sign-reversed wave with $\cos \rightarrow -\cos$. The permittivity coefficients $\{\ln \tilde{\epsilon}\}_n$ in Eq. (18) are determined by expanding $\ln[\tilde{\epsilon}[\cos[2\pi z/\lambda]]]$ as a series in cosine powers, then substituting with the exponential formula $\cos[2\pi z/\lambda] = (\exp[i2\pi z/\lambda] + 1/\exp[i2\pi z/\lambda])/2$, and collecting common exponential powers algebraically using Mathematica (Wolfram 1991). ZP force modes are then calculated using Eq. (20) with the integral in Matsubara frequency ξ evaluated numerically. Both Mathematica and C++ were used in different formulations of the problem.

ZP pressure profiles for small amplitude permittivity waves all look qualitatively like the example shown here for $\Delta\epsilon_e/\langle\epsilon_e\rangle = 0.1$. They are dominated by the ZP modes \bar{F}_0 and \bar{F}_2 . ZP pressure profiles for larger permittivity contrasts do noticeably change in appearance as illustrated in Figure 7 for $\Delta\epsilon_e/\langle\epsilon_e\rangle = 0.5$. They exhibit an increased contribution from the ZP wave modes \bar{F}_1 and \bar{F}_3 , with even a significant contribution from the \bar{F}_4 mode. For both figures, model parameters representative of quartz are used: electronic transition frequency $\omega_e = 2\text{E}16 \text{ rad/s}$, plasma frequency $\omega_p = 0$, and mean static permittivity $\langle\epsilon_e\rangle = 3.5$.

These ZP pressure profiles are in close quantitative agreement with those obtained by a direct method with the reflection coefficients evaluated by numerical integration of Eq. (12) iterating from a zero prior approximation, followed by numerical integration of the ZP force in Eq. (4) abruptly truncated at the Compton frequency $\omega_x = \omega_C$. The direct method provides reasonably indistinguishable results within its noise levels. However direct methods are more limited as they exhibit a noise cross-talk between Fourier modes close to the machine precision, which still becomes evident as systematic deviations in single high n modes or in difference profiles.

Adding previous iterations of the reflection coefficient \tilde{R} back into the integral Eq. (12), even for permittivity waves as large as $\Delta\tilde{\epsilon} = \langle\tilde{\epsilon}\rangle$, introduces a change in the mode amplitudes \bar{F}_n no larger than 2% for

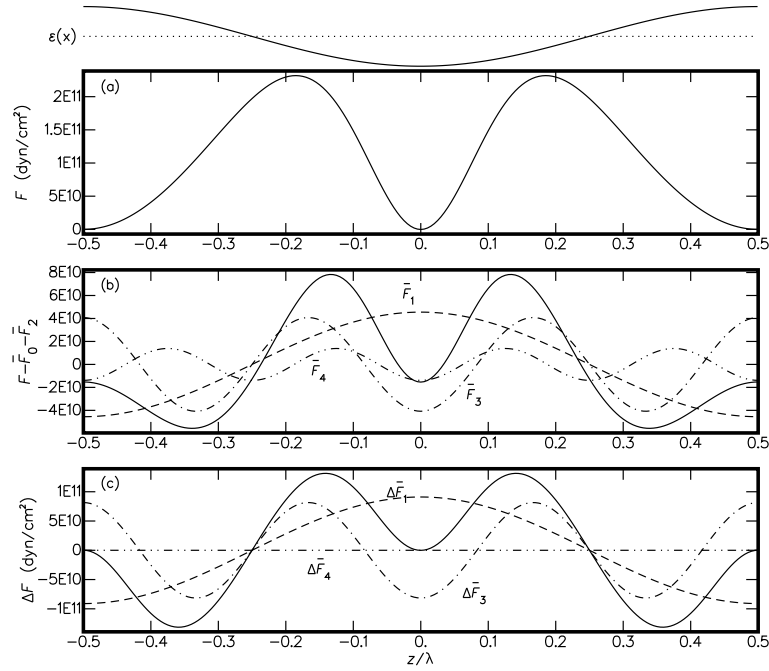


Figure 7: ZP pressure profiles as in Figure 6 but for a larger amplitude static-permittivity wave with relative contrast $\Delta\varepsilon_e/\langle\varepsilon_e\rangle = 0.5$.

the worst cases, at the smallest wavelengths $\lambda = \text{E}-9$ cm and in Fourier modes $n \gtrsim 30$. Introducing the denominator in the reflection terms produces relative changes of E-6 in the ZP force in the worst cases, and the perpendicular reflection terms \mathcal{R}_s produce no larger than an E-14 relative effect. Little change in the profiles is seen at wavelengths near the cutoff, suggesting that the solution is little affected by the form of the cutoff as with the use of a Lorentzian cutoff in the Fourier method. In all of the numerical solutions described in this paper, integrals are evaluated using Simpson's rule with at least 60 intervals over their ranges of maximum contribution. Increasing the number of intervals produces no significant changes $>1\%$ in the result. Inui (2008) has applied a direct computational implementation of a recursive formula for the reflection coefficients to estimate ZP pressures in linearly graded media.

In Figure 8, mode amplitudes $|2^{(n \neq 0)} \bar{F}_n|$ are shown for $\lambda = \text{E}-6.5$ cm, with a relative contrast of 0.5 in the four parameters, static permittivity ε_e , electronic transition frequency ω_e , plasma frequency ω_p , and Drude collision frequency γ_D . Characteristically $|\bar{F}_0| \simeq |2\bar{F}_2|$ and $|2\bar{F}_1| \simeq |2\bar{F}_3|$. Mode amplitudes drop off with a slope in n beyond $n = 3$ proportional to the relative contrast.

With the reversal in the sign of the permittivity wave, the main Fourier modes \bar{F}_0 and \bar{F}_2 , with all of the even n modes, do *not* change, and so vanish in the difference profile $\Delta F[z]$. Both of the next significant wave modes \bar{F}_1 and \bar{F}_3 , as well as all of the odd n modes, change sign, and so make up the difference profile $\Delta F[z]$.

Figure 9 shows ZP pressure mode amplitudes $|2^{(n \neq 0)} \bar{F}_n|$ as a function of wavelength λ in (a), and ZP pressure differences $|2\Delta\bar{F}_n|$ in (b), for a number of relative static-permittivity contrasts $\Delta\varepsilon_e/\langle\varepsilon_e\rangle$. The profiles run parallel with a slope $1/\lambda^2$, although there is some evidence for flattening in the slope in the odd modes for $\lambda \lesssim \text{E}-8.5$ cm approaching the Compton cutoff wavelength $\lambda_C = \text{E}-9.6$ cm. Flattening at small wavelengths in both odd and even modes is more evident in waves in other of the permittivity parameters (not shown). Separation between contrast groups $\Delta\varepsilon_e < \langle\varepsilon_e\rangle$ in the main Fourier modes \bar{F}_0 and \bar{F}_2 (solid) go as the relative permittivity contrast squared, \bar{F}_1 and \bar{F}_3 (dashed) as the contrast cubed, and \bar{F}_4 (dot-dashed) as the contrast to the fourth power.

The difference spectra in (b) show only the coinciding residuals \bar{F}_1 and \bar{F}_3 (dashed), which are separated

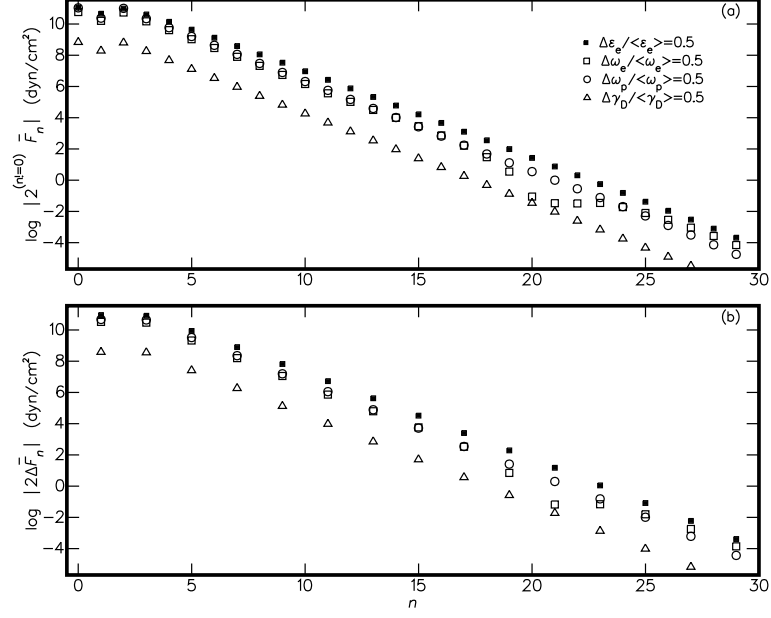


Figure 8: ZP cosine mode amplitudes $\log |2^{(n!=0)} \bar{F}_n|$ for the ZP pressure profile in (a), and for the difference profile $\log |2\Delta\bar{F}_n|$ in (b), for waves in the four permittivity parameters: static permittivity ϵ_e , electronic transition frequency ω_e , plasma frequency ω_p , and Drude collision frequency γ_D .

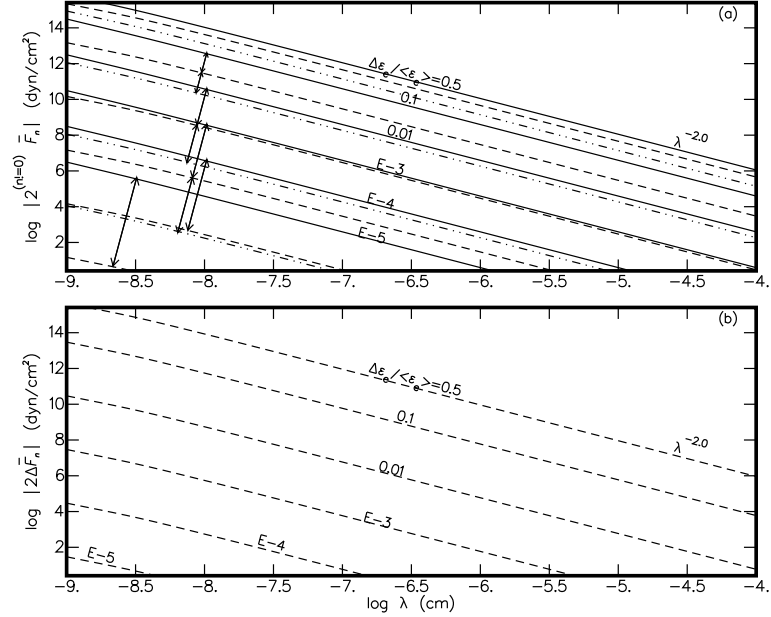


Figure 9: ZP cosine-mode amplitudes $\log |2^{(n!=0)} \bar{F}_n|$ in (a) and ZP pressure differences $\log |2\Delta\bar{F}_n|$ in (b) as functions of wavelength λ for different static-permittivity relative contrasts $\Delta\epsilon_e / \langle\epsilon_e\rangle$, showing the main coinciding modes $|\bar{F}_0| = |2\bar{F}_2|$ (solid), coinciding residuals $|2\bar{F}_1| = |2\bar{F}_3|$ (dashed), and $|2\bar{F}_4|$ (dot-dot-dashed). To distinguish overlapping modes, vectors are drawn connecting modes in each permittivity-contrast group.

by three orders of permittivity contrast between groups, indicating that the differences, like the modes themselves, go as the relative permittivity contrast cubed. Only the coinciding odd modes $\Delta\bar{F}_1$ and $\Delta\bar{F}_3$ appear in the difference spectra, since ZP modes for $n > 4$ are not shown.

Graded solutions for permittivity waves are overall repulsive with the ZP bulk mode \bar{F}_0 always positive, as the product in Eqs. (19) and (20) is negative, $(n - q)q\{\overline{\ln \tilde{\epsilon}}\}_{n-q}\{\overline{\ln \tilde{\epsilon}}\}_q = -q^2|\{\overline{\ln \tilde{\epsilon}}\}_q|^2 \leq 0$ for $n = 0$ and for all q , using the Hermitian property $\{\overline{\ln \tilde{\epsilon}}\}_{-q} = \{\overline{\ln \tilde{\epsilon}}\}_q^*$. For a permittivity wave $\rho_{\tilde{p}}[z] \sim \cos[2\pi z/\lambda]$ of relatively small amplitude, so that $\tilde{R}_{\tilde{p}\pm}[z]$ can be ignored in the solution Eq. (12) of the differential Eq. (10), smoothly varying reflection coefficients are antisymmetric $R_{\tilde{p}+}[z] = -R_{\tilde{p}-}[z]$ at relatively high wavenumbers $\kappa \gg \pi/\lambda$ or high frequencies $\omega/c \gg \pi/\lambda$, which leads to a repulsive ZP force. Repulsive solutions are similarly found with soft boundaries modeled by permittivity gradients (Podgornik & Parsegian 2004; Philbin et al. 2010).

ZP modes above some n , as $n > 1$ in the examples of Figures 6 and 7, dip negatively at the lows and highs in the permittivity, which adds an attractive component that may offset the repulsive force in more picket-fence-like periodic permittivity waveforms. In the examples described in this section, the ZP mode \bar{F}_1 is anticorrelated with the permittivity wave and attractive at the wave bottom. It may act to either pump-up or dissipate a longitudinal acoustic wave depending upon the sign of the acousto-optic effect for the material.

5 Piezo-ZP Energy Dynamics

The mechanical energy transfer in a bulk piezoelectric medium associated with acoustic waves is determined by a total energy U in a stressed piezo crystal with the energy increment (Mason 1966)

$$dU = T_{ij}dS_{ij} + E_i dD_i, \quad (23)$$

summing over repeated indices in a term, with the usual stress T_{ij} and strain S_{ij} symmetric 3×3 tensors containing both longitudinal ($i = j$) and transverse ($i \neq j$) effects, and the electric field E_i and electric displacement D_i 3-element spatial vectors. Indices count coordinates $i = x, y, z$; x_i denotes the spatial coordinate $(x_x, x_y, x_z) \equiv (x, y, z)$.

For a developed example of the phenomenology of ZP energy coupling, the present work is limited to nonconducting piezo materials in a bulk medium with no changes of state over their ranges of variation. The total energy U from (23) is then conserved, $dU = 0$, with the ZP forced mechanical work $T_{ij}dS_{ij}$ balancing the capacitive energy loss $-E_i dD_i$.

Material parameters are assumed to be linearly coupled supposing small variations, and thus connected by two constitutive relations, with the most convenient pair for this work written (Ikeda 1990, Table 2.1)

$$\begin{aligned} T_{ij} &= c_{ijpq}S_{pq} - h_{pj}D_p, \\ E_i &= -h_{ijp}S_{jp} + \epsilon_{ij}D_j, \end{aligned} \quad (24)$$

with the elastic stiffness at constant electric displacement c_{ijpq} a $3 \times 3 \times 3 \times 3$ tensor, which is defined using the inverse of the material compliance tensor s_{ijpq} , with the impermeability at constant strain ϵ_{ij} a 3×3 matrix, and with the piezoelectric constant h_{ijp} a $3 \times 3 \times 3$ tensor, which enters symmetrically between the material response for the converse piezo effect in the first equation in (24) and the voltage response for the normal piezo effect in the second equation.

Stress-caused energetic processes do not give a capacitive transfer when the ZP mechanical work $T_{ij}dS_{ij}$ done over a cycle vanishes, with the stress T_{ij} and strain S_{ij} varying in phase. Then the electric field E_i and electric displacement D_i both must also vary in phase for $dU = 0$ in Eq. (23), and in phase with the stress and strain, as is evident from the constitutive relations (24). A transfer of energy between the ZP mechanical and dielectric terms occurs if integrals of $T_{ij}dS_{ij}$ or $E_i dD_i$ over a cycle are nonzero. If the stress leads the strain, the integral of TdS is positive, and ZP mechanical work is converted into dielectric energy. The stress may lag the strain too, corresponding to the transfer from an external electrical supply into ZP opposed mechanical motions.

The ZP pressure $F[z, t]$ in a permittivity wave is described as a longitudinal z traction force of expansion acting inside the material, and so is represented in the force-balance equation (Auld 1973, Sections 2.B and 2.C)

$$\rho \frac{\partial^2 u_i}{\partial t^2} - \frac{\partial T_{ij}}{\partial x_j} = -\frac{\partial F[z, t]}{\partial z} \delta_{iz}, \quad (25)$$

with ρ the density of the medium, and u_i the particle-displacement 3 vector.

Particle displacements define the strain tensor

$$S_{ij} = \frac{1}{2} \left(\frac{\partial u_i}{\partial x_j} + \frac{\partial u_j}{\partial x_i} \right). \quad (26)$$

For consistency with the forcing, 1D solutions are studied with $\partial/\partial x = \partial/\partial y = 0$ everywhere in the interior of the crystal, which gives ZP force driving equations for the three nonvanishing nonredundant strain elements S_{xx} , S_{yz} , and S_{zz} ; as S_{ij} is symmetric, $S_{zx} = S_{xz}$ and $S_{zy} = S_{yz}$. Taking the z derivative of (25) yields

$$\rho \frac{\partial^2 S_{zz}}{\partial t^2} - \frac{\partial^2 T_{zz}}{\partial z^2} = -\frac{\partial^2 F[z, t]}{\partial z^2}, \quad (27)$$

and for $i = x, y$

$$2\rho \frac{\partial^2 S_{iz}}{\partial t^2} = \frac{\partial^2 T_{iz}}{\partial z^2}. \quad (28)$$

Using the first constitutive relation in (24) to eliminate the tension terms in the force equations (27) and (28) yields the strain for a given ZP force F and electric displacement D_i ; for S_{zz}

$$\rho \frac{\partial^2 S_{zz}}{\partial t^2} - (c_{zzjz} + c_{zzzj}) \frac{\partial^2 S_{jz}}{\partial z^2} = \frac{\partial^2}{\partial z^2} (-F[z, t] - h_{jzz} D_j), \quad (29)$$

and for S_{xz} and S_{yz}

$$2\rho \frac{\partial^2 S_{iz}}{\partial t^2} - (c_{izjz} + c_{izzj}) \frac{\partial^2 S_{jz}}{\partial z^2} = -h_{jiz} \frac{\partial^2 D_j}{\partial z^2}. \quad (30)$$

The three coupled linear differential equations (29) and (30) are wave equations for the forcing F in three nonzero independent strain and three electric-displacement elements. The first equation is in the direction of the vector forcing, and leads to a particular solution having the generic form

$$\bar{S}[k_z] = \frac{k_z^2}{k_z^2 - k_S^2} (s\bar{F}[k_z] + sh\bar{D}[k_z]), \quad (31)$$

for the scalar strain S and electric displacement D , which are tensor and vector amplitudes in specific directions appropriate to the overall solution. The wave equation is written in Fourier space taking $\partial^2/\partial t^2 \rightarrow -4\pi^2\nu^2$, and $\partial^2/\partial z^2 \rightarrow -4\pi^2k_z^2$ with $\bar{S}[k_z]$, $\bar{F}[k_z]$ and $\bar{D}[k_z]$ functions of k_z , the z element of the wavenumber in cycles per cm, which is related to the dimensionless integer wavenumber n of Section 3 as $k_z = n/\lambda$. An effective constant scalar converse piezo coefficient is denoted h , and constant scalar material compliance s , which is the relevant component of the inverse of the elastic stiffness at constant electric displacement c_{ijpq} . The characteristic wavenumber is defined $k_S = \nu(s\rho)^{1/2}$, for $1/(s\rho)^{1/2}$ the wave phase speed at vibration frequency ν with ρ the material density; k_S represents the vibration wavenumber for the frequency ν of the ZP forcing.

Strictly, piezo coupling may occur at resonance with $k_z = k_S$ for a vanishing denominator in Eq. (31), but acoustic waves with wavelength smaller than the dimensions of the crystal will produce a piezo fluctuating voltage with zero sum effect. Energy transfer with small piezos, comparable in size to the acoustic wavelength, has been demonstrated experimentally (Wang et al. 2007), but for macroscopic piezos, only a bulk modulation produces a single-signed voltage effect, which even gives a summed total voltage with incoherent contributions from independent waves through the piezo volume.

In the case where $k_S = 0$ as for the ZP bulk forcing, the multiplier in Eq. (31) becomes 1 over the entire Fourier domain (including at $k_z = 0$ by L'Hospital's rule), and transforming back to the spatial domain gives

a strain response $S = sF + shD$. The ZP bulk force contributes to the strain directly in the term sF , and indirectly with the added converse piezo contribution shD , which is both relatively small and phase shifted, being of relative amplitude the piezo coupling coefficient (Ikeda 1990, Section 2.6). The bulk strain solution corresponds to the static response $T = F$, referring to the constitutive relation (24). A static piezo response is typically assumed for slow piezo processes usual in energy-harvesting applications.

A spatially periodic permittivity wave of arbitrary shape of wavelength λ and frequency ν traveling in $\pm z$ with speed $\lambda\nu$ is represented by the translation $z/\lambda \rightarrow z/\lambda \mp \nu t$, in each term in the Fourier series in (17). The translation passes through into the ZP force in the series' Eqs. (14) and (22), without changing the Fourier modes \bar{F}_n in Eq. (19). As simply expected, the ZP force travels at velocity $\pm\lambda\nu$ with the permittivity wave. Just as the \bar{F}_0 bulk mode in the unmoving wave is spatially constant, in the traveling wave it is also temporally constant, and does not produce a net piezo energy transfer.

A standing permittivity wave is obtained by the superposition of equal-amplitude oppositely directed $\pm z$ traveling waves, represented by the translation

$$e^{i2\pi n \frac{z}{\lambda}} \rightarrow \frac{1}{2} \left(e^{i2\pi n (\frac{z}{\lambda} - \nu t)} + e^{i2\pi n (\frac{z}{\lambda} + \nu t)} \right) = \frac{1}{2} e^{i2\pi n \frac{z}{\lambda}} (e^{-i2\pi n \nu t} + e^{i2\pi n \nu t}) = e^{i2\pi n \frac{z}{\lambda}} \cos[2\pi n \nu t],$$

in each term of the Fourier series (17). In the superposition a cosine factor containing the time dependence is adjoined to each mode. A purely sinusoidal wave in the log of the permittivity is defined by just the two nonzero $n = \pm 1$ Fourier modes, which gives a Fourier series for the reflection coefficient also with only the two nonzero modes $R_{(p\pm)n}$ with $n = \pm 1$ in Eq. (18), but a ZP force with three nonzero modes \bar{F}_0 and $\bar{F}_{\pm 2}$ from the products between pairs of Fourier terms in Eq. (19). The temporal factors multiply in the ZP force modes yielding $\cos[2\pi n \nu t] \cos[2\pi n' \nu t] = \cos[2\pi \nu t]^2 = (1 + \cos[4\pi \nu t])/2$ in all the product combinations between mode pairs $n = \pm 1$ and $n' = \pm 1$, irrespective of their signs. A uniform temporal modulation of the three ZP modes \bar{F}_0 and $\bar{F}_{\pm 2}$ from 1 to 0 to 1, or from on to off to on, at the frequency 2ν is introduced, as was suggested in Figure 3 in the introduction. In a nonsinusoidal wave in the log of the permittivity with more than just the $n = \pm 1$ Fourier terms, all of the ZP modes, including the bulk \bar{F}_0 , become modulated with differing temporal factors of more complicated form.

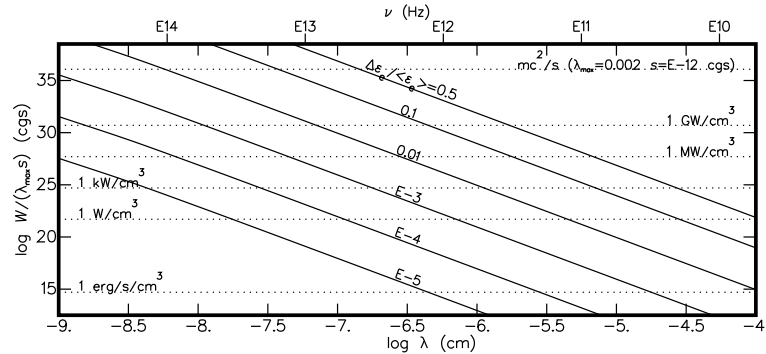


Figure 10: Available ZP power W per unit of crystal volume as a function of wavelength λ in a standing permittivity wave of relative contrast $\Delta\varepsilon_e/\langle\varepsilon_e\rangle$ with quartz acoustic frequency ν (on top). Power levels are shown for quartz (dotted).

In acting in an elastic body of total length L , a ZP bulk pressure \bar{F}_0 produces a dimensionless strain $s\bar{F}_0$, which increases the body length by $s\bar{F}_0L$, where s is a representative elastic compliance for the material. The ZP force does net work through the length of the elastic body L enlarging it by a continuous motion. As the ZP force changes in time t as in Figure 3 from $\bar{F}_0[t=0.25/\nu] = 0$ to its extreme value $\bar{F}_0[t=0.5/\nu] = \bar{F}_0$ (not necessarily linearly), it does a total work defined as the integral of $\bar{F}_0[t]$ times the infinitesimal expansion distance $sL\partial\bar{F}_0[t]$ over the ZP force range from 0 to its maximum \bar{F}_0 , which gives the total work done per unit of surface area $sL\bar{F}_0^2/2$ in terms of the maximum force \bar{F}_0 . Thus the total piezo power transfer or energy per unit of time and volume over the two permittivity half-wave cycles in each full acoustic wave

cycle becomes

$$W = \lambda_{\max} s \nu \bar{F}_0^2. \quad (32)$$

including the piezo energy-transmission coefficient $\lambda_{\max} < 1$, which is needed as the maximum realizable stress-strain phase shift possible limits the maximum power that can actually be transferred in a given material (Ikeda 1990, Sections 2.1 and 2.6.2).

Power estimates are shown in Figure 10 using the ZP force profiles from Section 4, with the static permittivity $\varepsilon_e = 3.5$ for quartz. The frequency $\nu = v_s/\lambda$ scale (shown on top) is for the quartz sound speed $v_s = 5.8\text{E}5$ cm/s. A representative quartz material compliance $s = 1\text{E}-11$ Pa $^{-1} = 1\text{E}-12$ cm 2 /dyn and energy-transmission coefficient $\lambda_{\max} = 0.002$ are used for the horizontal power levels. Power levels for piezo conversion are extremely high for quartz biphonon lattice vibrations $\nu \simeq 20$ THz = E13.3 Hz or $\lambda = \text{E}-7.6$ cm, far in excess of megawatts per cm 3 , even for a relative contrast $\Delta\varepsilon_e/\langle\varepsilon_e\rangle = 1\text{E}-3$, which is safely below crystal damage levels. At that frequency, power levels reach a mass/energy equivalent in less than 0.1 seconds for even an amplitude of oscillation $\Delta\varepsilon \lesssim 0.1\langle\varepsilon\rangle$!

The voltage difference between electrodes is defined by the electric field, the order of which is determined by the piezo relation $E \simeq gT \simeq g\bar{F}_0$, for $g = sh$ the piezoelectric voltage constant; for quartz $g \simeq 7\text{E}-5$ Volt cm/dyn. The voltage difference E increases in proportion to \bar{F}_0 , whereas the maximum power goes as \bar{F}_0^2 , so the maximum current also goes as \bar{F}_0 . For a relative static-permittivity contrast $\Delta\varepsilon_e/\langle\varepsilon_e\rangle = 1\text{E}-3$ with $\nu = 20$ THz and $\lambda = \text{E}-7.6$ cm in Figure 9, the ZP bulk force is $\bar{F}_0 = \text{E}8$ dyn/cm 3 , which produces an electric field $E = 7\text{E}3$ V/cm, still somewhat less than the atmospheric breakdown electric field for arcing.

6 Discussion

The Casimir effect, the attraction of discrete parallel conducting plates in a vacuum due to quantum ZP fluctuations characteristically weakens from a $1/\ell^3$ dependence to a $1/\ell^4$ retarded dependence as the plate separation increases through $\ell \simeq \text{E}-6.2$ cm = 6.3 nm, and weakens further at still larger separations $\ell \gtrsim \text{E}-4$ cm = 1 μm with a drop off that steepens with increasing temperature. The Casimir ZP force in a stack of discrete plates of alternating permittivity always follows closely the properties of a single pair of plates, as the ZP force at every location in a stack is determined by the most nearby plates.

The ZP force in a medium with a *smoothly* varying permittivity is found to exhibit no temperature dependencies. For a given repeating profile with spatial scales of variation always larger than the light wavelength for the frequency cutoff, the ZP force decreases universally as the inverse square $1/\lambda^2$ of the wavelength λ . In a sinusoidal wave it is repulsive. In a static-permittivity wave of wavelength $\lambda = \text{E}-7.6$ cm = 2.5Å, it is about 400 times stronger than the Casimir ZP force in the corresponding discrete alternating-layer stack of the same repetition scale and static-permittivity contrast, comparing Figures 9a and 12a. The ZP force is stronger in a stack of discrete perfectly conducting plates in alternate layers, but weakens dramatically with more realistic conductivities comparing with Figure 12c, and falls off much more rapidly with larger repetition scale anyway.

The main reason that the ZP force in a medium of smoothly varying permittivity differs so markedly from that in a stack of discrete plates is that with a smoothly varying permittivity the ZP force is most affected by the *highest* frequency ZP fluctuations, whereas with finite permittivity steps it is determined by the *lowest* frequency ZP fluctuations. ZP fluctuations are exponentially attenuated across a constant permittivity layer, which leads to a low-frequency cutoff in finite permittivity steps. On the other hand, the main ZP force contribution in a graded permittivity comes from near the high-frequency cutoff for a divergent quantum integral, which is taken to be the Compton electron-photon scattering frequency, as permittivity effects arise with electronic states. A very high light-frequency cutoff corresponding to the scale of Compton scattering seems physically justified, since a graded permittivity should be smoothly changing only up to the photo-electric interaction scale, as the material substance is actually described by spatially discrete electronic oscillators.

The ZP force in a permittivity wave ranges from near zero at the wave extrema to a maximum repulsive force in the most sloping portions of the wave, represented by two most significant equal-amplitude harmonics of bulk repulsive dc \bar{F}_0 and double wavenumber \bar{F}_2 . With larger amplitudes of oscillation, additional

harmonics may become significant too, including the mode \bar{F}_1 , which matches the acoustic wave itself in wavenumber and phase. In a medium with a correct sign of acousto-optic effect, the \bar{F}_1 mode may be able to pump up and sustain a longitudinal acoustic wave or lattice vibration if it is excited above some minimal amplitude.

In a traveling acoustic wave, the ZP bulk force \bar{F}_0 remains constant, but in a standing wave it is modulated at twice the acoustic wave frequency. If an acoustic wave is standing and coherent in finite domains through the volume of a piezo crystal as with biphonon lattice vibrations, the bulk mode may be significantly modulated and couple piezoelectrically with an external electrical dc load through end electrodes perpendicular to the wave direction, as in the illustrated ‘crystal power’ layout of Figure 2. A transfer of electrical energy out of the ZP fluctuating field is predicted with the possibility of extremely high power levels as summarized in Figure 10. In an acoustic wave of frequency 20 THz, in the range of biphonon lattice vibrations in quartz, estimated power levels reach a mass energy equivalent mc^2 in a crystal mass m of stimulated domains in less than 0.1 seconds with a relative permittivity contrast still $\lesssim 0.1$ or a relative index-of-refraction contrast $\lesssim 0.3$.

Acknowledgements

It is the author’s contention that specific clues for this work have been Divinely given. The author wishes that the guidance, concepts, and designs for the extraction of energy from the ZP field described here remain unpatentable, but stay in the public domain.

Appendices

A Alternating-Layer Stack

Figure 11 illustrates ZP pressure as a function of spatial repetition scale $\lambda = 2\ell$ in an alternating-layer stack with equal layer thicknesses. The $\Theta = 0\text{K}$ calculations are derived by integrating numerically in Eq. (4), and the three-layer calculations for three nonzero temperatures by evaluating the Matsubara sum from (1); the Lifshitz asymptotic power-law line F_- is taken from (37) and F_+ from (38) in Appendix B. The three-layer (solid line) closely follows the relatively small-scale F_- and large-scale F_+ asymptotic power laws. The multilayer 0K solution ($n_\ell = 20$, long-dashed) deviates slightly. Temperature effects become important for repetition scales $\lambda \gtrsim \text{E-4 cm} = 1\mu\text{m}$.

For all the numerical models described in this paper, a usual form for the complex permittivity as a function of light frequency ξ is adopted

$$\varepsilon[\xi] = 1 + \frac{\varepsilon_e - 1}{1 - (\xi/\omega_e)^2} - \frac{\omega_p^2}{(\xi + i\xi_0)(\xi + i\gamma_D)}, \quad (33)$$

which represents a single electronic band at frequency ω_e of strength $\varepsilon_e - 1$, and an added conductive effect for the plasma frequency ω_p , with the Drude collision frequency γ_D . A small base frequency ξ_0 is included for numerical calculations.

The static permittivity ε_e is the permittivity at zero frequency $\xi = 0$ in a nonconductor $\omega_p = 0$; $\varepsilon_e = 3.5$ for quartz. The permittivity at the high frequency extreme exhibits the limit $\varepsilon[\xi \rightarrow \infty] = 1$, which is found to be applicable even in generalized conductivity models that include contributions from free electrons (Klimchitskaya et al. 2009). Characteristically the highest electronic transition is most important for ZP forces $\omega_e \simeq 2\text{E16 rad/s}$, corresponding to the Rydberg frequency $\omega_e = m_e e^4 / \hbar^3 / 2$, for m_e the electron rest mass and e the elementary charge. A lattice vibration band at around 9E12 rad/s in crystals is the next lower-frequency effect, but is of relatively small oscillator strength to make a significant contribution. The plasma frequency ω_p ranges from 0 to 2E15 rad/s in semiconductors, and reaches about 1.6E16 rad/s in doped semiconductors or in the best room-temperature metallic conductors; in normal thick conductors $\gamma_D \simeq 2\text{E14 rad/s}$. In numerical calculations with a nonzero plasma frequency ω_p , integrals are started a

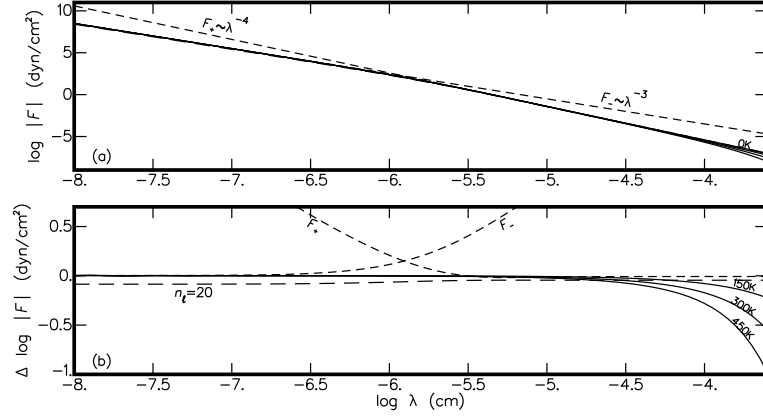


Figure 11: ZP pressure as a function of repetition length $\lambda = 2\ell$, from $1\text{E}-8\text{ cm} = 1\text{\AA}$ to $\text{E}-3.6\text{ cm} = 2.5\mu\text{m}$, in an alternating static permittivity of relative contrast $\Delta\varepsilon_e/\langle\varepsilon_e\rangle = 0.01$, for 3 layers for $\Theta = 0\text{K}$ and three $\Theta > 0\text{K}$ temperatures (solid lines), and for 41 layers for 0K ($n_\ell = 20$, long-dashed), compared with asymptotic power laws F_- and F_+ (dashed). ZP pressure with $\log F$ for 3 layers at 0K subtracted is shown in (b) on a magnified ZP pressure scale.

little above $\xi = 0$ or a small base frequency $\xi_0 \lesssim \text{E}3\text{ rad/s}$ is introduced to avoid infinities at $\xi = 0$, which are procedures that only insensitively affect the results.

Due to the Kramers-Krönig causality constraints, the complex permittivity is real on its imaginary frequency axis consistent with the projected $\tilde{\varepsilon}[\xi] \equiv \varepsilon[i\xi]$ from Eq. (33)

$$\tilde{\varepsilon}[\xi] = 1 + \frac{\varepsilon_e - 1}{1 + (\xi/\omega_e)^2} + \frac{\omega_p^2}{(\xi + \xi_0)(\xi + \gamma_D)}. \quad (34)$$

The projected real permittivity is a slowly decreasing monotonic function of frequency ξ ; it is plotted in many places for conductors or nonconductors (e.g. Klimchitskaya et al. 2009, Figure 20).

The parametric representation in (33) and (34) is taken to remain applicable over the range of permittivity change. Thus small permittivity changes $|\Delta\tilde{\varepsilon}|$ around the average $\langle\tilde{\varepsilon}\rangle$, $|\Delta\tilde{\varepsilon}| \ll \langle\tilde{\varepsilon}\rangle$, can be represented by the derivative expansion

$$\Delta\tilde{\varepsilon} = \frac{\partial\tilde{\varepsilon}}{\partial\varepsilon_e}\Delta\varepsilon_e + \frac{\partial\tilde{\varepsilon}}{\partial\omega_e}\Delta\omega_e + \frac{\partial\tilde{\varepsilon}}{\partial\omega_p}\Delta\omega_p + \frac{\partial\tilde{\varepsilon}}{\partial\gamma_D}\Delta\gamma_D. \quad (35)$$

Figure 11 illustrates the ZP pressure that arises with variations in the static permittivity between even and odd layers $\varepsilon_{e0} = \langle\varepsilon_e\rangle - \Delta\varepsilon_e$ and $\varepsilon_{e1} = \langle\varepsilon_e\rangle + \Delta\varepsilon_e$, with $\langle\varepsilon_e\rangle = 3.5$ and $\Delta\varepsilon_e = 0.01\langle\varepsilon_e\rangle$, for $\omega_e = 2\text{E}16\text{ rad/s}$ in a nonconductor $\omega_p = 0$.

Figure 12 shows the ZP pressure $F[\lambda]$ alternating the static permittivity in (a) around $\langle\varepsilon_e\rangle = 3.5$, with $\omega_e = 2\text{E}16\text{ rad/s}$ and $\omega_p = 0$, the electronic transition frequency in (b) around $\langle\omega_e\rangle = 2\text{E}16\text{ rad/s}$, with $\varepsilon_e = 3.5$ and $\omega_p = 0$, and the plasma frequency in (c) between $\omega_{p0} = 0$ in nonconducting even layers and ω_{p1} in conducting odd layers, using $\gamma_D = 2\text{E}14\text{ rad/s}$ and $\varepsilon_e = 1$ supposing the ideal of evacuated nonconducting layers for illustration. In all of the examples, only quite small changes are seen with more than a minimal number of layers $n_\ell \gtrsim 1$. Shifting the spatial phase by one layer thickness, that is interchanging the even and odd layers, produces very small differences, which go only as third order or less in the permittivity contrast.

Symmetric multilayer stacks all follow the thin limit for the three-layer sandwich solutions discussed in Appendix B, going as $1/\lambda^3$ or $1/\ell^3$. However the spatially varying electronic transition frequency ω_e in (b) exhibits a different definite thick-layer power law for retarded solutions going as $1/\ell^8$ rather than the $1/\ell^4$ predicted for usual circumstances, as discussed in Appendix B. For all relative static-permittivity contrasts, the ZP force in an alternating layer stack of repetition scale $\lambda = \text{E}-7.6\text{ cm} = 2.5\text{\AA}$ is only about $1/400$ that found in the corresponding sinusoidal permittivity wave, comparing ZP pressures between Figures 12a and 9a.

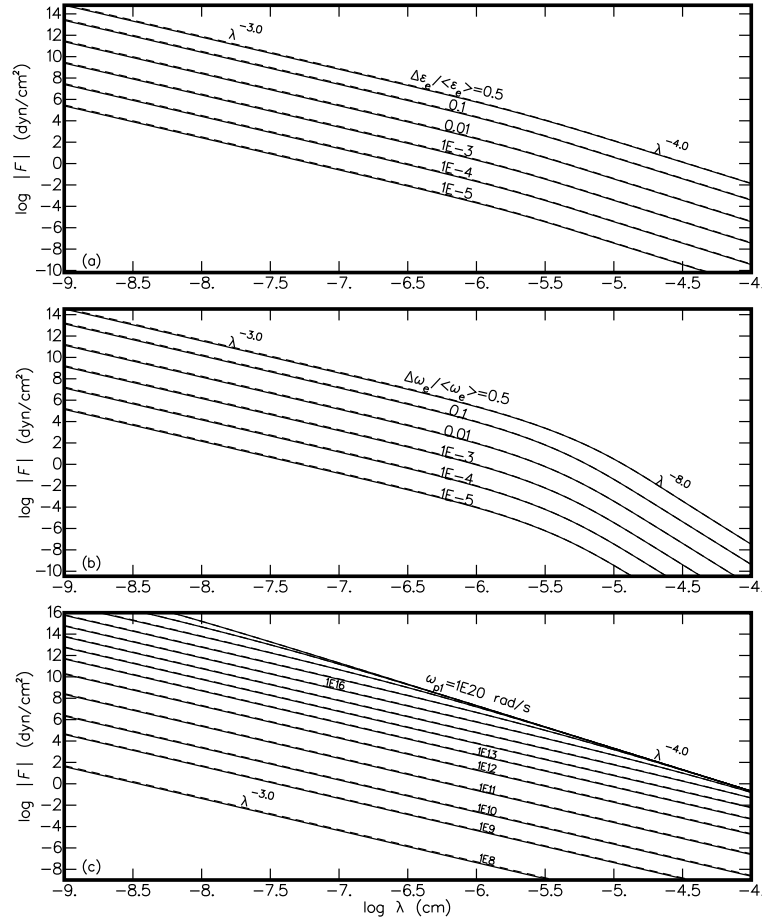


Figure 12: ZP pressure $F[\lambda = 2\ell]$ with different relative contrasts, alternating in static permittivity ε_e in (a), electronic transition frequency ω_e in (b), and plasma frequency with ω_{p1} in odd layers in (c). Calculations are shown for 41 nearby layers ($n_\ell = 20$, solid) and the minimum case of 3 layers ($n_\ell = 1$, dashed).

The ZP force increases with relative permittivity contrast, going as $(\Delta\varepsilon_e/\langle\varepsilon_e\rangle)^2$ in (a), and as $(\Delta\omega_e/\langle\omega_e\rangle)^2$ in (b), with deviations no larger than 0.5% in relative strength $\Delta F/F$ over the range of repetition scales up to relative contrasts 0.01. The ZP force follows a squared dependence since the frequency integrals are over terms $R_{\tilde{p}}^+[\succ\frac{\ell}{2}]R_{\tilde{p}}^-[\prec\frac{\ell}{2}]$ as in (8), where $R_{\tilde{p}}^+[\succ\frac{\ell}{2}] \sim r_{\tilde{p}}^-[\frac{-\ell}{2}]$ and $R_{\tilde{p}}^-[\prec\frac{\ell}{2}] \sim r_{\tilde{p}}^+[\frac{\ell}{2}]$ from the innermost jump, with $r_{\tilde{p}}^\pm[\pm\frac{\ell}{2}] \sim \Delta\tilde{\varepsilon}/\langle\tilde{\varepsilon}\rangle$ from Eq. (6) for small permittivity contrasts as in the derivatives for graded media in (11).

ZP forces for alternating plasma frequencies ω_{p1} in 12c all follow thin asymptotic $1/\ell^3$ power laws up to a scale $\lambda = 2\ell$, where the solution joins the upper $1/\ell^4$ limiting power-law line. Solutions with higher plasma frequencies $\omega_p > E20$ rad/s follow essentially this limiting solution line, which corresponds closely to the Casimir-predicted perfect-conductivity limiting form in Eq. (39).

Using repetition length $\lambda = \ell_0 + \ell_1$ to characterize alternating-layer stacks facilitates comparison with wavelength in a permittivity wave. The figures show only alternating-layer calculations with $\ell_0 = \ell_1 = \ell = \lambda/2$, as the Casimir ZP force with differing even- and odd-layer thicknesses is determined essentially by the even (middle-) layer thickness alone, and exhibits little change with increasing relative thickness above some minimal $\ell_1 \lesssim \ell_0$. Likewise, the ZP force exhibits only a weak dependence upon the number of layers n_ℓ used in the calculation, with deviations no larger than 0.01 in $\log F$ or 2.3% in relative strength over the

range of repetition scales ($\Delta F/F = \Delta \log F/\log e$). The interfacial-reflection contributions from jumps in the reflection coefficients $R_{\beta\pm}[z]$ in a multilayer stack are increasingly exponentially attenuated with increasing distance from the middle $z = 0$ layer in Eq. (7).

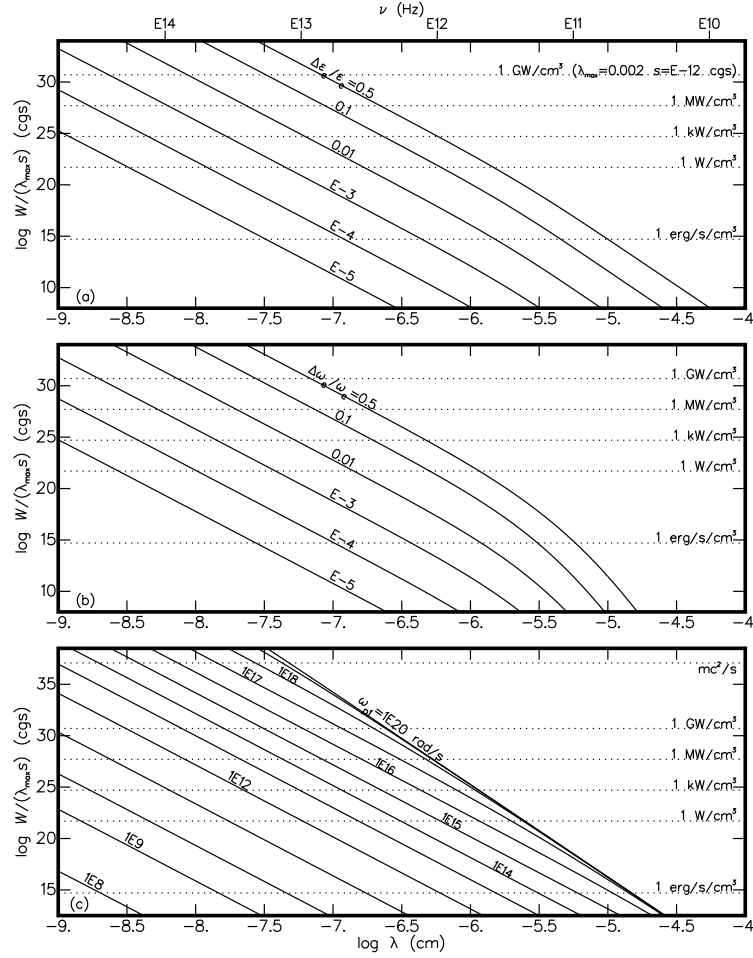


Figure 13: Available ZP power W per unit of crystal volume as a function of repetition length $\lambda = 2\ell$ in a stack with alternating static permittivity in (a), electronic transition frequency in (b), and plasma frequency in (c), supposing a modulation frequency $\nu = v_s/\lambda$ with $v_s = 5.8E5$ cm/s, showing power levels (dotted).

Figure 13 shows estimates for the available ZP power in alternating layer stacks. Nominally a modulation frequency $\nu = v_s/\lambda$ (shown on top) with speed $v_s = 5.8E5$ cm/s is adopted representative of quartz, but power levels scale in proportion to frequency for schemes that modulate layers at a different frequency. For an alternating conductivity in (c), levels are adjusted downward slightly to take account of intermediate quartz piezos in even layers with $\epsilon_{e0} = 3.5$ unmodulated in permittivity.

Power estimates are for cycling the permittivity state at a rate ν rather than 2ν , and so follow the permittivity-wave formula Eq. (32) divided by 2. Also since the plasma frequency is cycled only in odd layers with a passive quartz piezo in between for (c), only half the volume participates in the energy extraction, so those power estimates follow the permittivity-wave formula Eq. (32) divided by 4. The material compliance $s = 1E-11$ Pa $^{-1} = 1E-12$ cm 2 /dyn and energy-transmission coefficient $\lambda_{\max} = 0.002$ are used for the horizontal power levels for quartz or typical piezo materials.

The available power goes like the square of the ZP force and so drops quite rapidly with increasing λ , and also depends quite strongly on the relative permittivity contrast in (a) and (b) going as the fourth

power. The most favorable power estimates are found with the plasma-frequency modulation in (c). For the example described in the introduction, a perfect conductor with intermediate quartz piezos shows an available power of about 3.5 kW/cm³ for $\lambda = E-6 \text{ cm} = 10 \text{ nm}$, or $\ell = 5 \text{ nm}$, modulated at the nominal frequency $\nu = 5.8E11 \text{ Hz}$. The higher modulation frequency $\nu = E13 = 10 \text{ THz}$ gives an available power that scales up to about 60 kW/cm³. However power levels fall off very rapidly with less-than-perfect conductivity. For more realistic conductivities for semiconductors with $\omega_p \lesssim 2E16$, the power level in the example drops to $<120 \text{ W/cm}^3$. Layers need to be considerably thinner for effects to become very appreciable.

B Asymptotic Three-Layer Solutions

The Lifshitz collaboration (Lifshitz 1956; Dzyaloshinskii et al. 1961) reports asymptotic forms for the ZP force in a three-layer stack for middle layers ℓ_0 thinner and thicker than a critical cross-over thickness $\ell_{\pm} \simeq c/(\omega_e \sqrt{\varepsilon_{e0}})$, for layers still thinner than the light wavelength for the Matsubara base frequency where temperature becomes important; ε_{e0} is the static permittivity or $\sqrt{\varepsilon_{e0}}$ the index of refraction in the middle layer. The highest frequency for permittivity change is the electronic transition frequency ω_e , supposing a lower plasma frequency $\omega_p < \omega_e$ in Eq. (34). Above that frequency the permittivity becomes asymptotic $\varepsilon \rightarrow 1$ and light waves are unretarded. The cross-over scale ℓ_{\pm} is the smallest wavelength for light travel in the medium for which retardation effects are seen, and thus determines the minimum layer thickness for the so-called ‘retarded’ solutions. In this section derivations for the limiting profiles are described and results discussed in the context of permittivity variations due to different of the permittivity parameters from Eq. (34).

The ZP force integral (4) is limited in its frequency range due to the exponential attenuation factor $\exp[-2\kappa_0 \ell_0]$, which appears in the reflection terms (2) in the product of reflection coefficients in a layer ℓ_0 of constant permittivity in Eq. (8). When the middle layer of a three-layer stack is sufficiently thin $\ell_0 < c/(\omega_e \sqrt{\varepsilon_{e0}})$, the corresponding critical wavenumber from the exponential factor is large $\kappa_0 = 1/\ell_0 > \omega_e \sqrt{\varepsilon_{e0}}/c$. Such large wavenumbers change relatively little between layers j , as the wavenumber $\kappa_j[\xi, \omega] = (\tilde{\varepsilon}_j[\xi]\xi^2 + \omega^2)^{1/2}/c$ is either determined by a frequency $\omega \gtrsim \omega_e$, which is the same between layers j , or by a Matsubara frequency $\xi \gtrsim \omega_e$ above the highest frequency for significant permittivity $\tilde{\varepsilon}_j[\xi]$ change. With a spatially constant wavenumber, the interfacial reflections at the permittivity jumps $r_{s\pm}[\pm \frac{\ell_0}{2}]$ from (6) become negligible, and the perpendicular s reflection coefficient $R_{s\pm}[\pm \frac{\ell_0}{2}]$ and reflection term \mathcal{R}_s can be ignored. Wavenumbers κ_j divide out in the parallel p polarization interfacial reflections leaving just the permittivities $\tilde{\varepsilon}_j[\xi]$ in $r_{p\pm}[\pm \frac{\ell_0}{2}]$ from (6).

Dropping the product of reflection coefficients from the denominator of \mathcal{R}_p in (2), as it is fourth-order in the relative permittivity contrast compared to the main second-order effect, leaves the only κ_0 dependence under the integral in the term $\eta^2 \exp[-2\eta]$, taking $\eta = \kappa_0 \ell_0$ to be a substitute variable of integration for ω as in Eq. (9). As the permittivity $\tilde{\varepsilon}_j[\xi]$ does not depend upon ω , it does not depend upon its substitute independent variable η , and the integrals separate leaving for the η integral the Gamma function $\int_0^\infty \eta^2 e^{-2\eta} d\eta = \frac{1}{4}$, then

$$F_- = -\frac{\hbar}{8\pi^2 \ell_0^3} \int_0^\infty \left(\frac{\Delta \tilde{\varepsilon}[\xi]}{\langle \tilde{\varepsilon}[\xi] \rangle} \right)^2 d\xi, \quad (36)$$

which is the Lifshitz thin-layer negative or compressive ZP pressure written for permittivities symmetric about a middle layer $j = 0$ (Dzyaloshinskii et al. 1961, Eq. (4.18)). The permittivity amplitude of variation $\Delta \tilde{\varepsilon}[\xi] = (\tilde{\varepsilon}_1[\xi] - \tilde{\varepsilon}_0[\xi])/2$, and average $\langle \tilde{\varepsilon}[\xi] \rangle = (\tilde{\varepsilon}_0[\xi] + \tilde{\varepsilon}_1[\xi])/2$, are used for consistency with Figure 4, with a symmetric arrangement $\tilde{\varepsilon}_1[\xi] = \tilde{\varepsilon}_{-1}[\xi]$ for layers numbered 0, ± 1 .

If the relative permittivity variation arises due to a varying static permittivity between layers $\varepsilon_{e\uparrow}$ in $\tilde{\varepsilon}[\xi]$ in Eq. (34), with the permittivity amplitude of variation $\Delta \tilde{\varepsilon} = (\partial \tilde{\varepsilon}[\xi]/\partial \varepsilon_e) \Delta \varepsilon_e = \Delta \varepsilon_e / (1 + (\xi/\omega_e)^2)$, and average $\langle \tilde{\varepsilon}[\xi] \rangle = (\tilde{\varepsilon}[\xi; \varepsilon_e \rightarrow \langle \varepsilon_e \rangle - \Delta \varepsilon_e; \omega_p \rightarrow 0] + \tilde{\varepsilon}[\xi; \varepsilon_e \rightarrow \langle \varepsilon_e \rangle + \Delta \varepsilon_e; \omega_p \rightarrow 0])/2 = 1 + (\langle \varepsilon_e \rangle - 1)/(1 + (\xi/\omega_e)^2)$, the ξ integral in (36) can be evaluated yielding

$$F_- = -\frac{\hbar \omega_e \sqrt{\varepsilon_e}}{32\pi \ell_0^3} \left(\frac{\Delta \varepsilon_e}{\langle \varepsilon_e \rangle} \right)^2, \quad (37)$$

which is the limiting form shown in Figure 11.

The thin-layer asymptotic ZP pressure Eq. (36) for a varying plasma frequency ω_p with static permittivity $\varepsilon_e = 1$ exhibits a straightforward solution form too (not written out here). An unmanageable analytic integral is arrived at with a varying electronic transition frequency ω_e in a nonconductor $\omega_p = 0$, and a nonanalytic integral with a varying Drude collision frequency Γ_p with static permittivity $\varepsilon_e = 1$. Anyway the numerical examples from Figure 12 show that all these follow the asymptotic thin-layer power law $1/\ell_0^3$ for small ℓ_0 , although conductors exhibit a cross-over scale that varies greatly with plasma frequency ω_p .

When the middle layer is sufficiently thick $\ell_0 > c/(\omega_e\sqrt{\varepsilon_{e0}})$, the critical wavenumber from the exponential attenuation factor $\exp[-2\kappa_0\ell_0]$ is small $\kappa_0 = (\tilde{\varepsilon}_0[\xi]\xi^2 + \omega^2)^{1/2}/c < \omega_e\sqrt{\varepsilon_{e0}}/c$, and the integral is determined by low-frequency contributions near $\xi = \omega = 0$, but still above the Matsubara $m = 1$ frequency. If zero-frequency permittivity variations exist, then it seems a good approximation to suppose that the permittivity is constant in frequency and well approximated by its zero-frequency value $\tilde{\varepsilon}_j[\xi] \rightarrow \tilde{\varepsilon}_j[0]$. Following the Lifshitz approach, new dimensionless integration variables are substituted into the integral Eq. (4), $\hat{\xi} = \xi\ell_0\sqrt{\tilde{\varepsilon}_0[0]}/c$ for the frequency ξ , and $\hat{\omega} = \omega\ell_0/c$ for ω , which gives $\kappa_0 = (\hat{\xi}^2 + \hat{\omega}^2)^{1/2}/\ell_0$ for the ZP force in the middle layer. With the substitutions, all scale dependencies factor out of the integrals into an ℓ_0^4 external divisor. In a symmetric arrangement, only a weak dependence upon the zero-frequency relative permittivity contrast between the layers $\Delta\tilde{\varepsilon}[0]/\langle\tilde{\varepsilon}[0]\rangle$ is left in the jump reflection coefficients in the remaining integral, which leads to

$$F_+ = -\frac{\pi^2\hbar c}{240\sqrt{\tilde{\varepsilon}_0[0]}\ell_0^4} \left(\frac{\Delta\tilde{\varepsilon}[0]}{\langle\tilde{\varepsilon}[0]\rangle} \right)^2. \quad (38)$$

quoting the result from the Lifshitz collaboration (Dzyaloshinskii et al. 1961, Eq. (4.22)); ϕ_{dd} is a weak function of the permittivity ratio $\tilde{\varepsilon}_1[0]/\tilde{\varepsilon}_0[0] = (\langle\tilde{\varepsilon}[0]\rangle + \Delta\tilde{\varepsilon}[0])/(\langle\tilde{\varepsilon}[0]\rangle - \Delta\tilde{\varepsilon}[0])$, $\phi_{\text{dd}} \simeq 0.35$ for $\tilde{\varepsilon}_1[0]/\tilde{\varepsilon}_0[0] < 3$. For small permittivity contrasts $\Delta\tilde{\varepsilon}[0]/\langle\tilde{\varepsilon}[0]\rangle \ll 1$ as in the numerical examples shown in Appendix A, the permittivity ratio $\tilde{\varepsilon}_1[0]/\tilde{\varepsilon}_0[0]$ is always close to 1, so $\phi_{\text{dd}} = 0.35$. This ZP force F_+ limiting line is shown in Figure 11. Like what is seen in Figure 12b, the asymptotic thick-layer solution Eq. (38) does not necessarily apply to permittivity variations produced with a varying electronic transition frequency ω_e between layers, as those permittivity variations vanish at low frequency ξ .

Comparing with Figure 12c, the asymptotic formula Eq. (38) can be seen to apply too above some infinitesimal repetition period λ or middle-layer cross-over thickness ℓ_0 in perfect conductors idealized with $\omega_p \rightarrow \infty$, or above a finite cross-over thickness ℓ_0 that increases in normal conductors with decreasing ω_p , at least up to the Matsubara $m = 1$ thickness where temperature effects become important. With a divergent zero-frequency permittivity $\lim_{\xi \rightarrow 0} \tilde{\varepsilon}_{\pm 1}[\xi] \rightarrow \infty$, but with $\tilde{\varepsilon}_0[0] = \varepsilon_{e0}$, it follows $\tilde{\varepsilon}_1[0]/\tilde{\varepsilon}_0[0] \rightarrow \infty$ in a symmetric stack $\tilde{\varepsilon}_1[0] = \tilde{\varepsilon}_{-1}[0]$, giving $\phi_{\text{dd}} = 1$ (Dzyaloshinskii et al. 1961, Figure 10), and the permittivity contrast asymptotically becomes $\Delta\tilde{\varepsilon}[0]/\langle\tilde{\varepsilon}[0]\rangle = (\tilde{\varepsilon}_1[0]/\tilde{\varepsilon}_0[0] - 1)/(\tilde{\varepsilon}_1[0]/\tilde{\varepsilon}_0[0] + 1) \rightarrow 1$, implying

$$F_+ = \frac{\pi^2\hbar c}{240\sqrt{\varepsilon_{e0}}\ell_0^4}, \quad (39)$$

which contains the original Casimir (1948) solution for an evacuated middle layer with $\varepsilon_{e0} = 1$.

The retarded cross-over thickness between the two power laws ℓ_{\pm} is defined strictly by the relation $F_-[\ell_0=\ell_{\pm}] = F_+[\ell_0=\ell_{\pm}]$, which gives

$$\ell_{\pm} = 1.448 \frac{c}{\omega_e \varepsilon_e}, \quad (40)$$

substituting with Eqs. (37) and (38) for static-permittivity variations with $\Delta\tilde{\varepsilon}[0] = \Delta\varepsilon_e$ and $\langle\tilde{\varepsilon}[0]\rangle = \langle\varepsilon_e\rangle$. An extra index-of-refraction $\sqrt{\varepsilon_e}$ enters into the divisor in this integral solution compared to the critical cross-over thickness ℓ_{\pm} for the peak wavenumber under the integral introduced at the beginning of this section. For $\varepsilon_e = 3.5$ and $\omega_e = 2\text{E}16$ rad/s, $\ell_{\pm} = 6.20$ nm or $\lambda = 2\ell_{\pm} = 12.40$ nm = E-5.91 cm, which agrees with the intersection of the dashed lines seen in Figure 11 and the cross-over thickness between the two power laws in Figure 12a.

References

- Auld, B. 1973, *Acoustic Fields and Waves in Solids*, John Wiley & Sons, New York
- Bethe, H. A. 1947, The Electromagnetic Shift of Energy Levels, *Phys. Rev.*, 72, 339–341, ADS
- Birkeland, O. J. & Brevik, I. 2007, Feigel effect: Extraction of momentum from vacuum?, *Phys. Rev. E*, 76(6), 066605, DOI, ADS
- Born, M. & Wolf, E. 1980, *Principles of Optics: Electromagnetic Theory of Propagation, Interference and Diffraction of Light*, Pergamon Press, Oxford, 6th edition, ADS
- Caride, A. O., Klimchitskaya, G. L., Mostepanenko, V. M., & Zanette, S. I. 2005, Dependences of the van der Waals atom-wall interaction on atomic and material properties, *Phys. Rev. A*, 71(4), 042901, DOI, ADS
- Casimir, H. B. G. 1948, On the Attraction between Two Perfectly Conducting Plates, *Proc. K. Ned. Akad. Wet.*, 51, 793–795
- Casimir, H. B. G. & Polder, D. 1948, The Influence of Retardation on the London-van der Waals Forces, *Phys. Rev.*, 73, 360–372, DOI, ADS
- Cavalleri, G. & Spavieri, G. 1989, Friction in vacuo starting from 10^{13} eV, *Nuovo Cimento A*, 101, 213–223, DOI, ADS
- Cole, D. C. & Puthoff, H. E. 1993, Extracting energy and heat from the vacuum, *Phys. Rev. E*, 48, 1562–1565, DOI, ADS
- Cooke, M. 2007, Filling the THz gap with new applications, *Semiconductor Today*, 2, 39–43
- Dowling, J. P. 1989, The Mathematics of the Casimir Effect, *Math. Mag.*, 62, 324–331
- Dzyaloshinskii, I. E., Lifshitz, E. M., & Pitaevskii, L. P. 1961, The general theory of van der Waals forces, *Adv. Phys.*, 10, 165–209, DOI, ADS
- Ellingsen, S. A. 2007, Casimir attraction in multilayered plane parallel magnetodielectric systems, *J. Phys. A*, 40, 1951–1961, DOI, ADS
- Feigel, A. 2004, Quantum Vacuum Contribution to the Momentum of Dielectric Media, *Phys. Rev. Lett.*, 92(2), 020404, DOI, ADS
- Feynman, R. P. & Hibbs, A. R. 1965, *Quantum Mechanics and Path Integrals*, McGraw Hill Book Company, New York
- Forward, R. L. 1984, Extracting electrical energy from the vacuum by cohesion of charged foliated conductors, *Phys. Rev. B*, 30, 1700–1702, DOI, ADS
- Haisch, B. & Moddel, G. 27 May, 2008, Quantum vacuum energy extraction, US Patent, 7,379,286
- Henkel, C. & Joulain, K. 2005, Casimir force between designed materials: What is possible and what not, *Europhys. Lett.*, 72, 929–935, DOI, ADS
- Horsley, S. A. R. & Philbin, T. G. 2014, Canonical quantization of electromagnetism in spatially dispersive media, *New J. Phys.*, 16(1), 013030, DOI, ADS
- Hough, D. H. & White, R. A. 1980, The Calculation of Hamaker Constants from Lifshitz Theory with Applications to Wetting Phenomena, *Adv. Colloid Interface Sci.*, 14, 3–14
- Ikeda, T. 1990, *Fundamentals of Piezoelectricity*, Oxford Univ. Press, Oxford, New York, Tokyo

- Inui, N. 2003, The Casimir Energy of a Medium Containing a Permittivity Gradient, *J. Phys. Soc. Jpn.*, 72, 280–286, DOI, ADS
- Inui, N. 2008, Casimir Energy of the Evanescent Field between Inhomogeneous Dielectric Slabs, *J. Phys. Soc. Jpn.*, 77(8), 084001, DOI, ADS
- Jacobsson, R. 1965, Light Reflection from Films of Continuously Varying Refractive Index, in *Progress in Optics*, ed. E. Wolf, Vol. 5, J. Wiley and Sons, New York, 247–286
- Klimchitskaya, G. L., Mohideen, U., & Mostepanenko, V. M. 2009, The Casimir force between real materials: Experiment and theory, *Rev. Mod. Phys.*, 81, 1827–1885, DOI, ADS
- Lambrecht, A., Jaekel, M., & Reynaud, S. 1997, The Casimir force for passive mirrors, *Phys. Lett. A*, 225, 188–194, DOI
- Lekner, J. 2016, *Theory of Reflection: Reflection and Transmission of Electromagnetic, Particle and Acoustic Waves*, Springer, Switzerland, 2nd edition
- Lifshitz, E. M. 1956, The Theory of Molecular Attractive Forces Between Solids, *JETP*, 2, 73–83, ADS
- Lipkin, R. 1996, Thin-film mirror changes into a window, *Science News*, 149, 182, ADS
- Maclay, G. J. 2000, A design manual for micromachines using Casimir forces: Preliminary considerations, in *Space Technology and Applications International Forum*, ed. M. S. El-Genk, Vol. 504 of *AIP Conference Series*, AIP, Melville, New York, 1060–1065, DOI, ADS
- Mandl, F. & Shaw, G. 2010, *Quantum Field Theory*, 2nd Edition, John Wiley & Sons, New York
- Mason, W. 1966, *Crystal Physics of Interaction Processes*, Academic Press, New York, London
- Milonni, P. W. 1994, *The Quantum Vacuum, An Introduction to Quantum Electrodynamics*, Academic Press, Inc., San Diego, CA
- Milonni, P. W. & Lerner, P. B. 1992, Extinction theorem, dispersion forces, and latent heat, *Phys. Rev. A*, 46, 1185–1193, DOI, ADS
- Ninham, B. W. & Parsegian, V. A. 1970, van der Waals Interactions in Multilayer Systems, *J. Chem. Phys.*, 53, 3398–3402, DOI, ADS
- Peskin, M. E. & Schroeder, D. V. 1995, *An Introduction to Quantum Field Theory*, Perseus Books, New York
- Philbin, T. G., Xiong, C., & Leonhardt, U. 2010, Casimir stress in an inhomogeneous medium, *Ann. Phys. (N.Y.)*, 325, 579–595, DOI, ADS
- Pinto, F. 1999, Engine cycle of an optically controlled vacuum energy transducer, *Phys. Rev. B*, 60, 14740–14755, DOI, ADS
- Pinto, F. 2008, Membrane Nano-Actuation by Light-Driven Manipulation of van der Waals Forces: A Progress Report, in *Space Technology and Applications International Forum-STAIIF*, ed. M. S. El-Genk, Vol. 969 of *AIP Conference Series*, AIP, Melville, New York, 1111–1119, DOI, ADS
- Podgornik, R., Hansen, P. L., & Parsegian, V. A. 2003, On a reformulation of the theory of Lifshitz-van der Waals interactions in multilayered systems, *J. Chem. Phys.*, 119, 1070–1077, DOI, ADS
- Podgornik, R. & Parsegian, V. A. 2004, Van der Waals interactions in a dielectric with continuously varying dielectric function, *J. Chem. Phys.*, 121, 7467–7473, DOI, ADS

- Raabe, C., Knöll, L., & Welsch, D. G. 2003, Three-dimensional Casimir force between absorbing multilayer dielectrics, *Phys. Rev. A*, 68(3), 033810, DOI, ADS
- Schwinger, J., DeRaad, Jr., L. L., & Milton, K. A. 1978, Casimir effect in dielectrics, *Ann. Phys. (N.Y.)*, 115, 1–23, DOI, ADS
- Tomaš, M. S. 2002, Casimir force in absorbing multilayers, *Phys. Rev. A*, 66(5), 052103, DOI, ADS
- Wang, X., Song, J., Liu, J., & Wang, Z. L. 2007, Direct-Current Nanogenerator Driven by Ultrasonic Waves, *Science*, 316, 102–105, DOI, ADS
- Wolfram, S. 1991, *Mathematica: a system for doing mathematics by computer*, 2nd edition, Addison-Wesley Publishing Co. Inc., Advanced Book Program, Reading, MA, ADS
- Zhou, F. & Spruch, L. 1995, van der Waals and retardation (Casimir) interactions of an electron or an atom with multilayered walls, *Phys. Rev. A*, 52, 297–310, DOI, ADS